On Compensating Magnetometer Swing in UAV Magnetic Surveys

Callum Walter, Alexander Braun & Georgia Fotopoulos

callum.walter@queensu.ca; braun@queensu.ca;
georgia.fotopoulos@queensu.ca

Department of Geological Sciences and Geological Engineering
Queen's University
Kingston, Ontario, Canada

2020 EGU General Assembly – Vienna, Austria – May 4-8, 2020

UAV-Borne Magnetometry

Research Motivation

To reliably integrate two innovative technologies and provide a technical balance between the existing resolution and coverage capabilities of conventional magnetic surveying platforms

Platform

Multi-Rotor Unmanned Aerial Vehicle

Sensor

Lightweight, High-Resolution, Optically Pumped Magnetometer

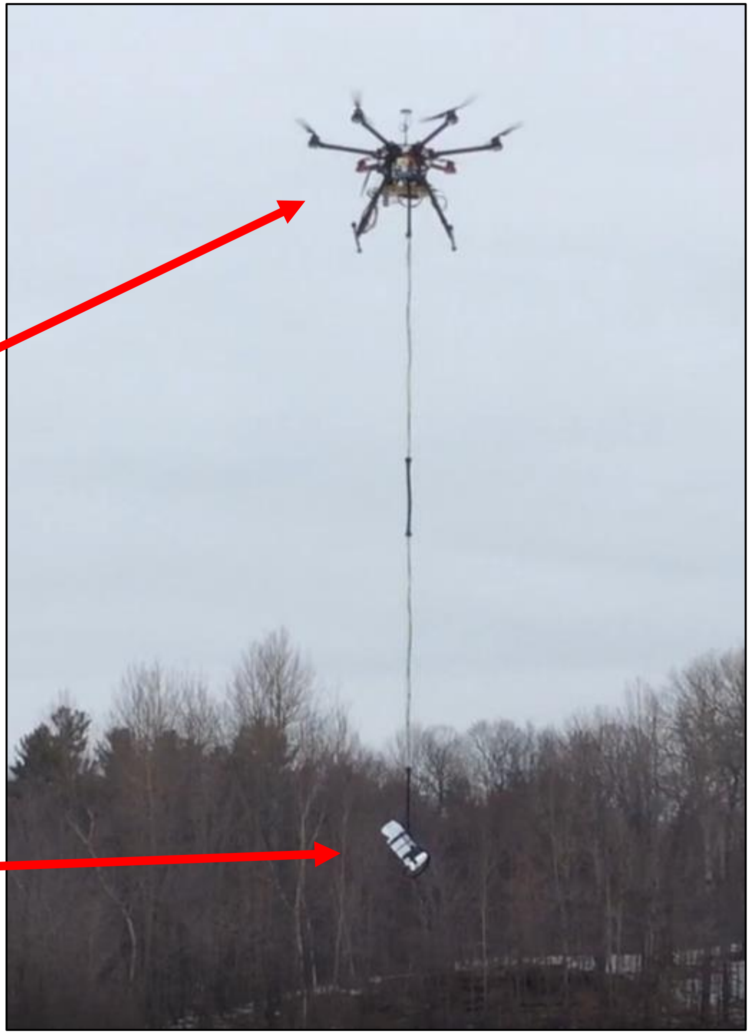

Walter et al. 2020

Conventional Magnetic Surveying Platforms

Manned Airborne

- Regional Survey Areas (>100 km^2)
- High Coverage Rate (>100 km/h)
- Relatively Low-Resolution Data

Terrestrial

- Localized Survey Areas (<10 km^2)
- Low Coverage Rate (<5 km/h)
- Relatively High-Resolution Data

Conventional Magnetic Surveying Platforms


C/O: Sander Geophysics Inc.

● Manned Airborne

● Terrestrial

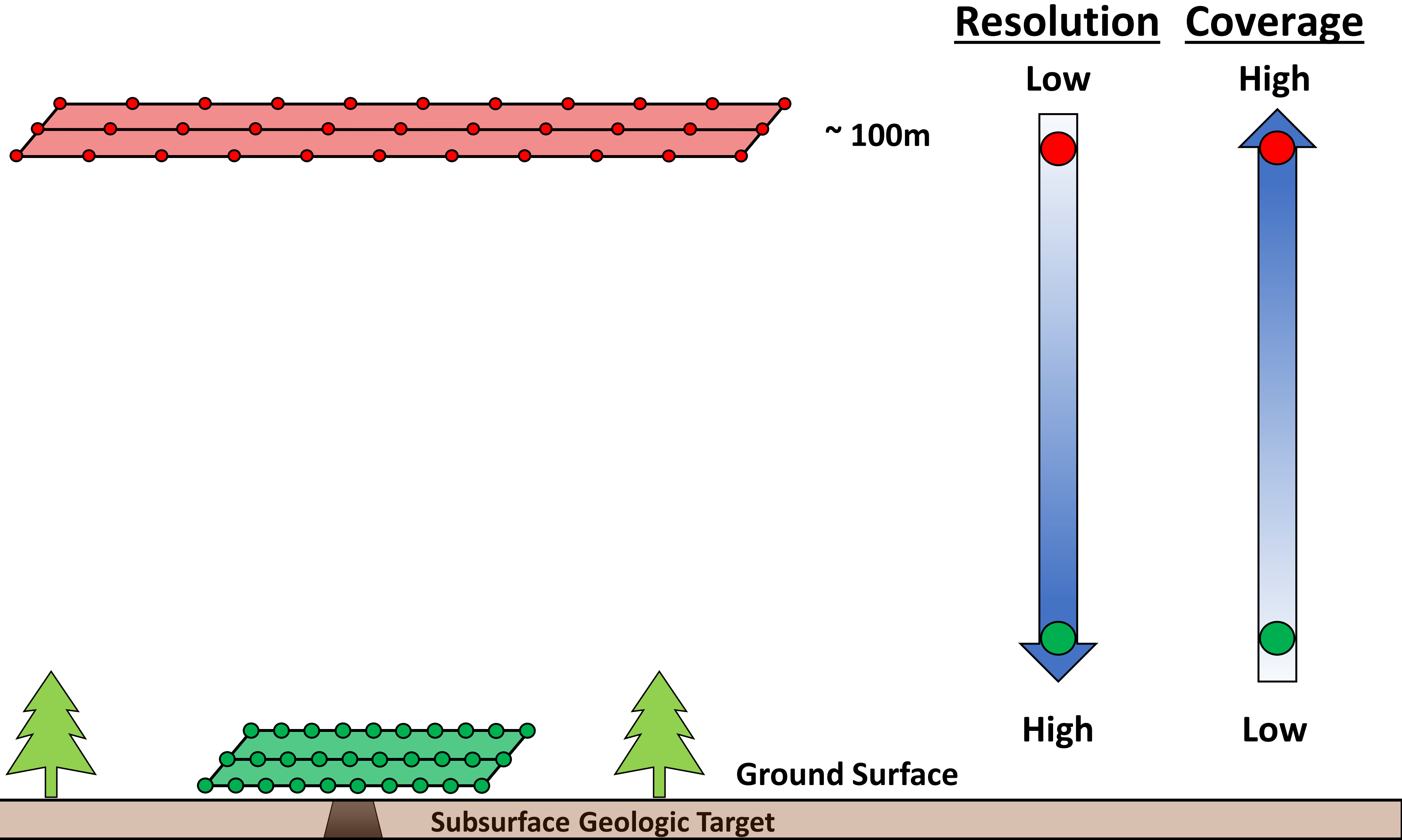

UAV-Borne Aeromagnetic Surveying Platforms

Manned Airborne

UAV-Borne

Terrestrial

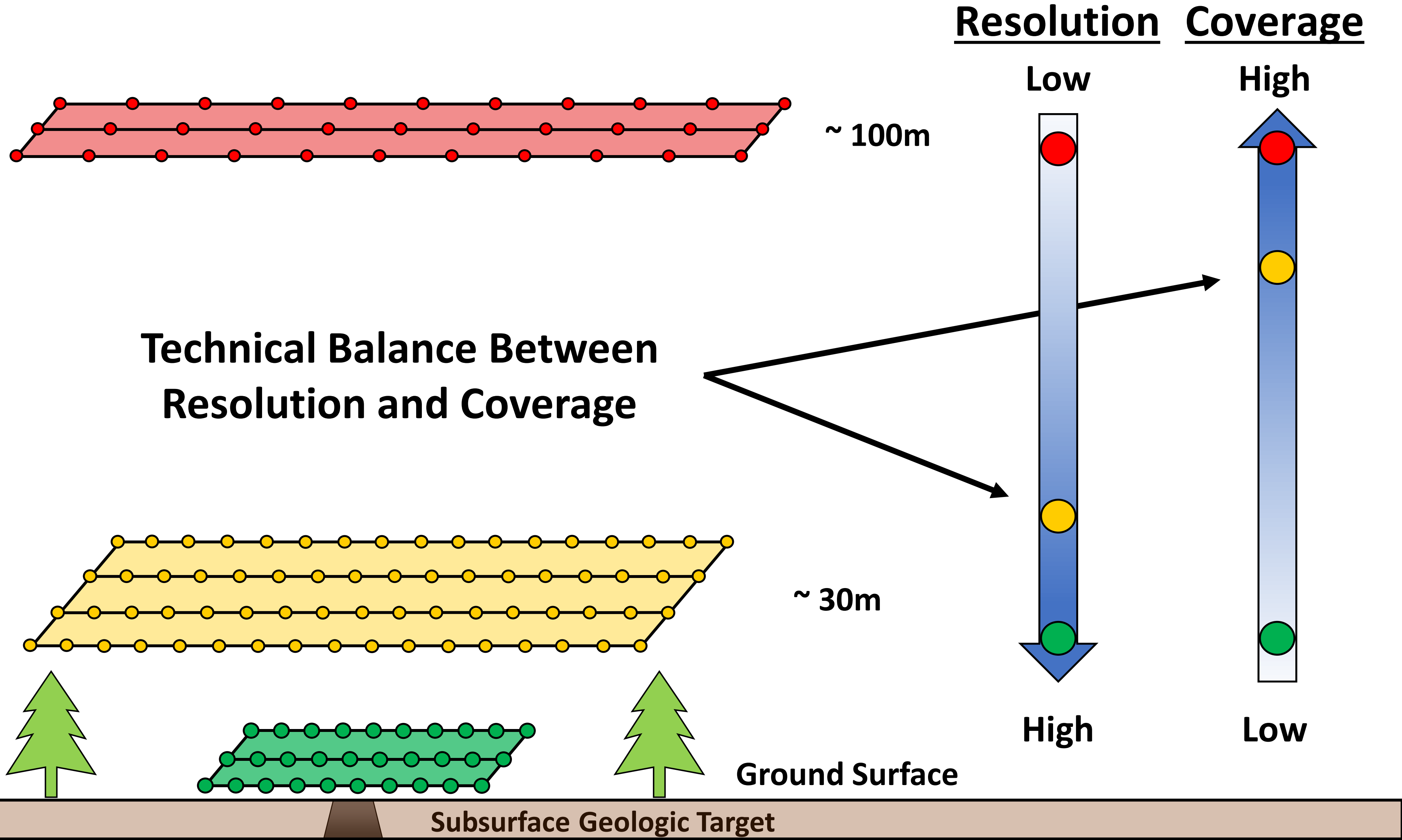

UAV-Borne Aeromagnetic Case Study

Published Manuscript: (1) Walter et al. 2020 - Geophysical Prospecting

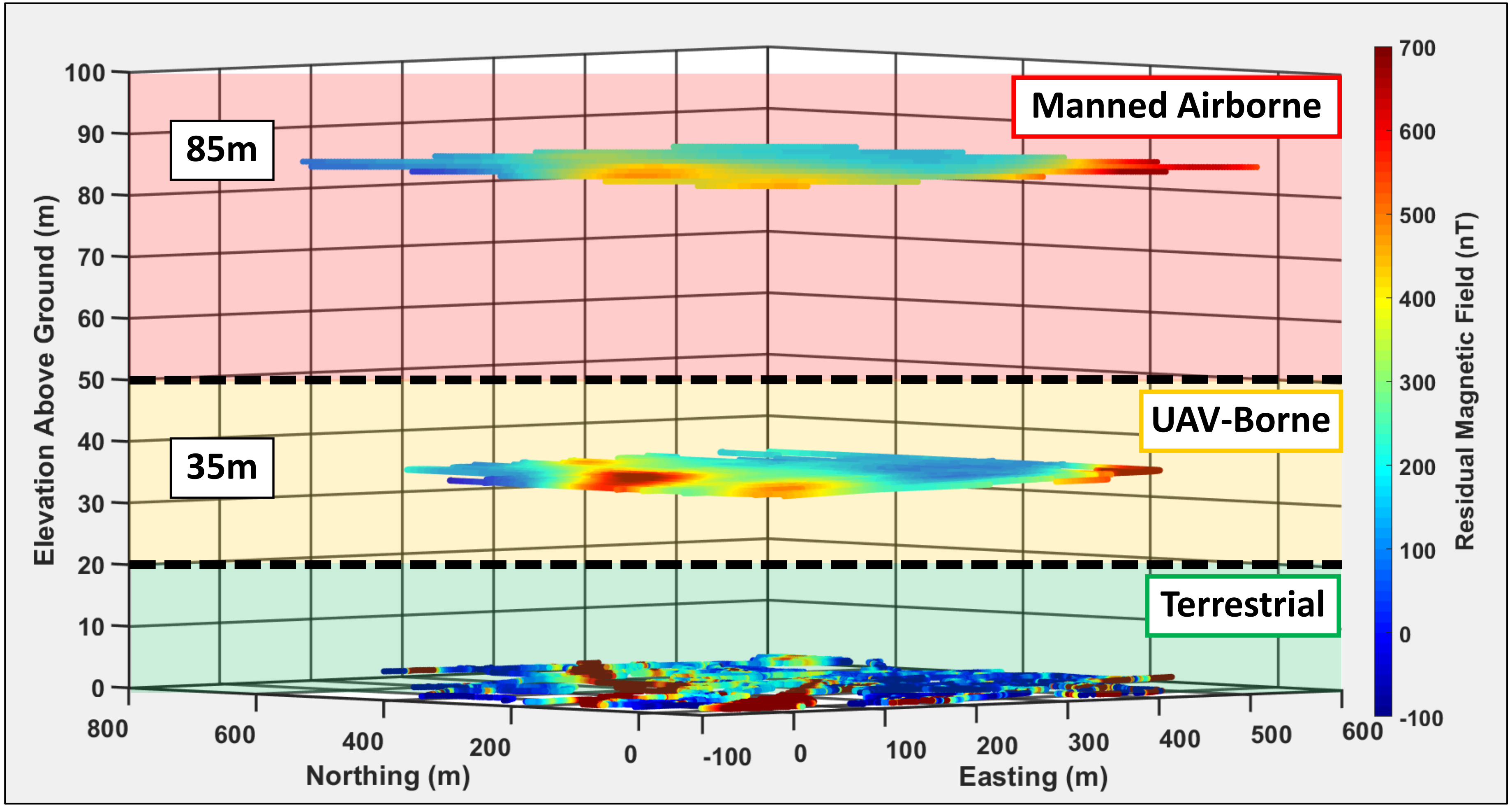

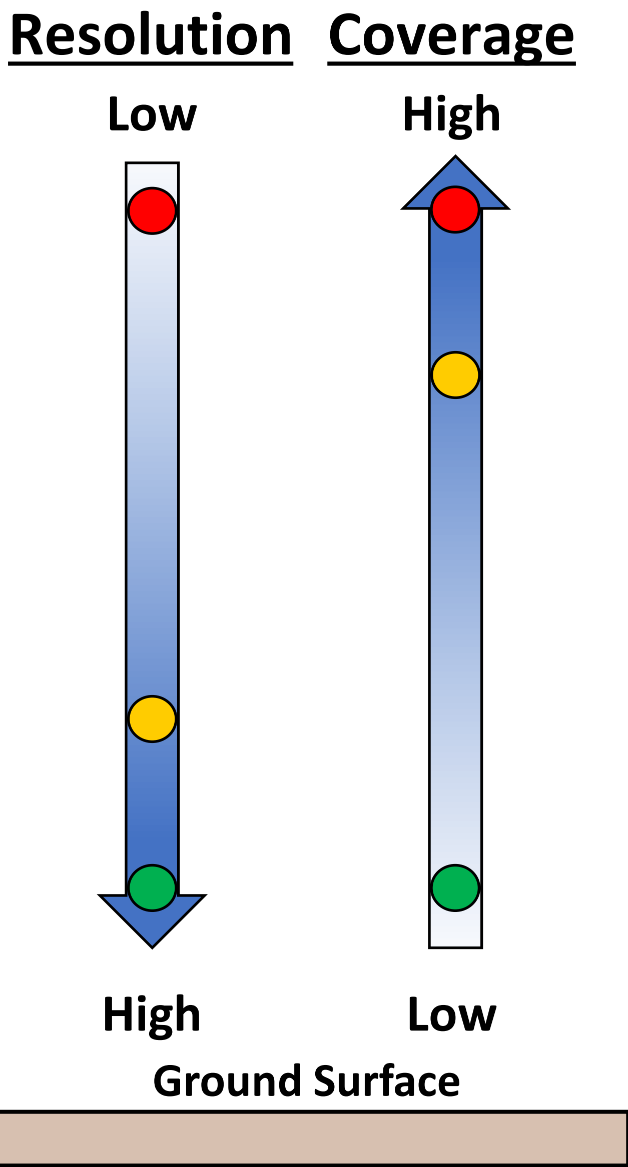

Integration of the Semi-Rigidly Suspended Magnetometer

DJI S900
Multi-Rotor UAV

GEM Systems - GSMP 35U
Potassium Vapour Magnetometer

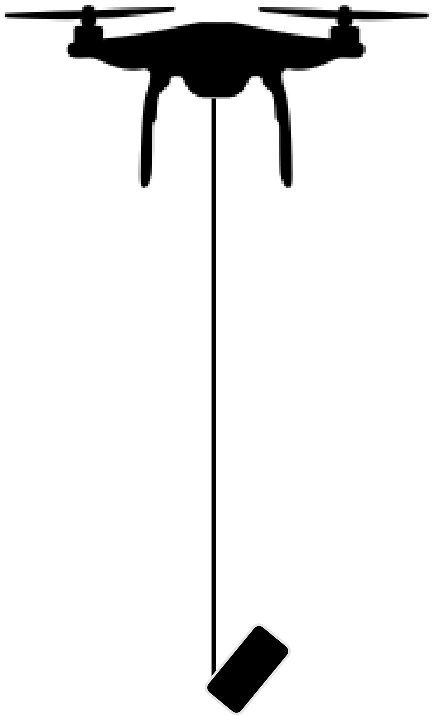

UAV-Borne
Aeromagnetic System

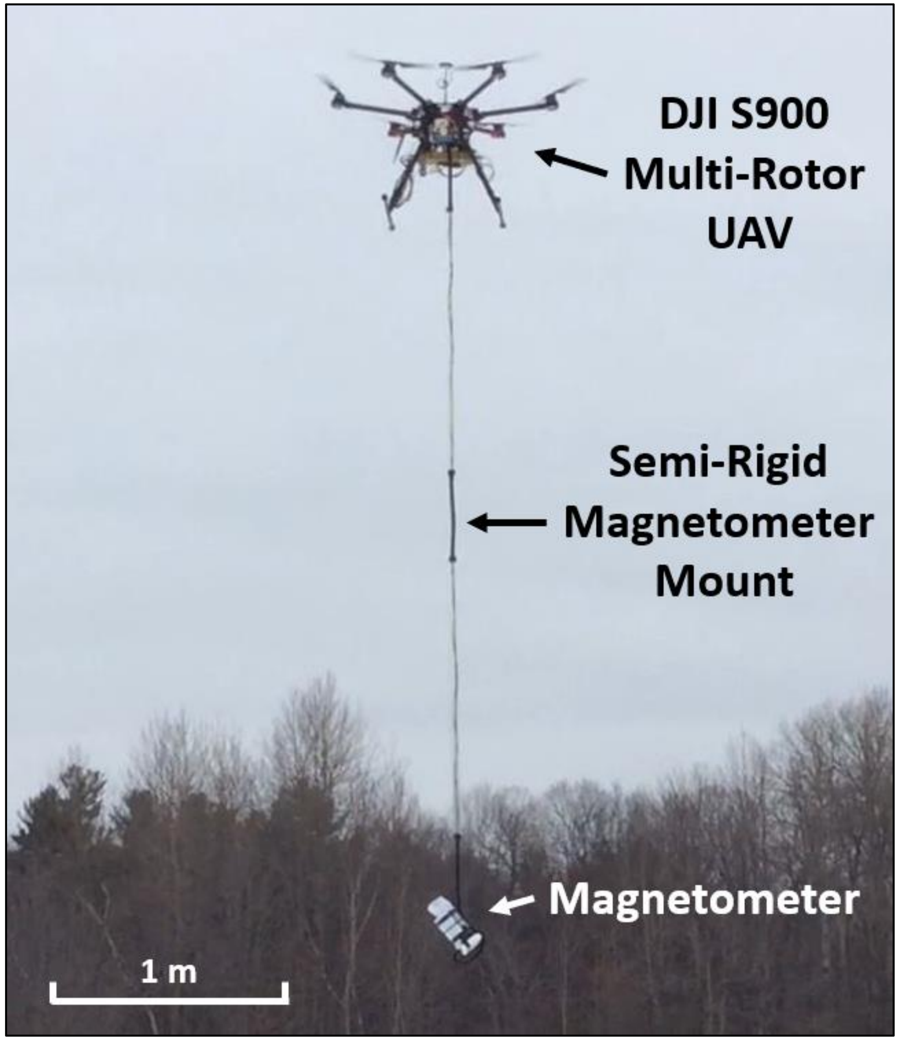

Critical Integration Consideration: Magnetic Interference Signals

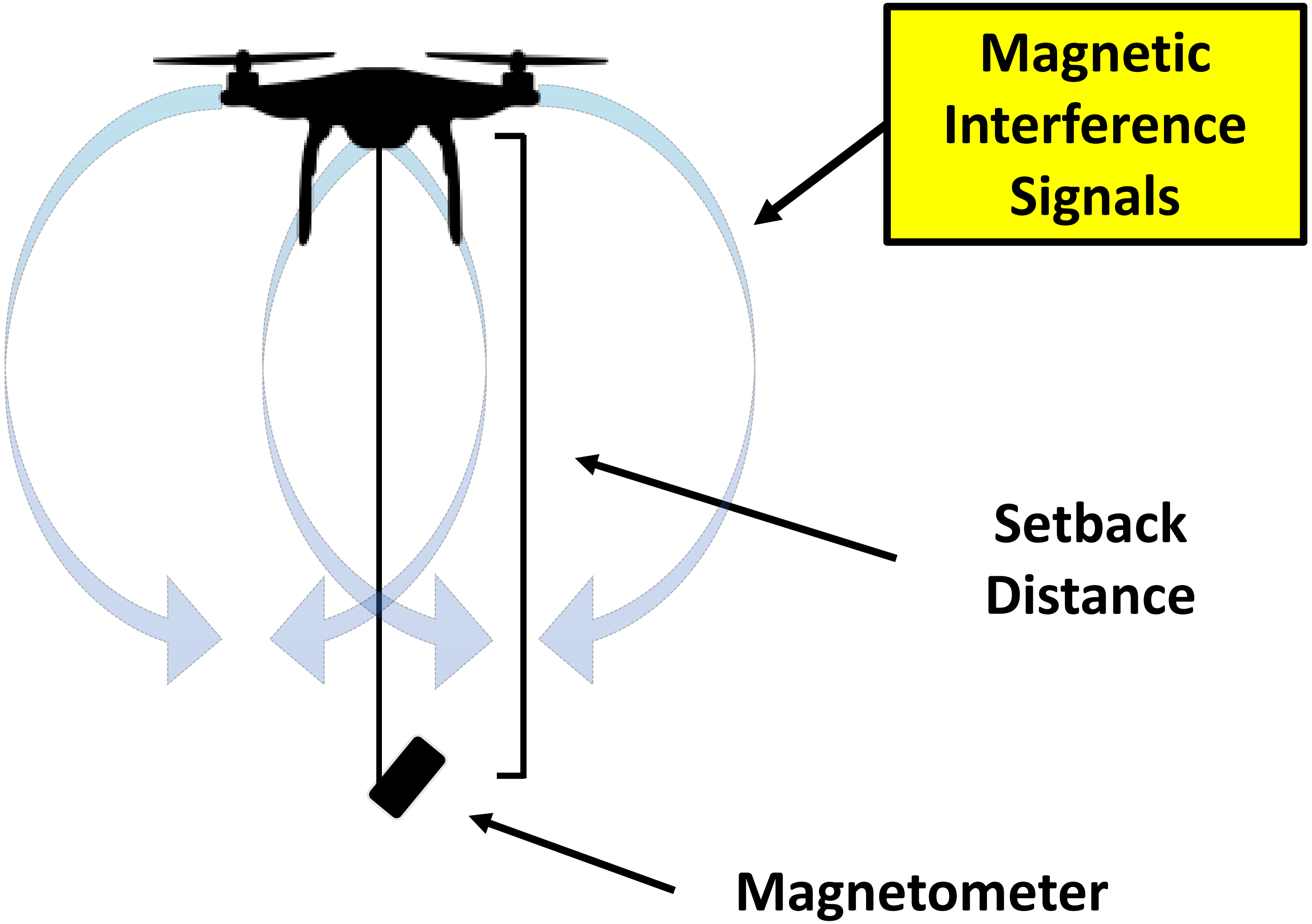

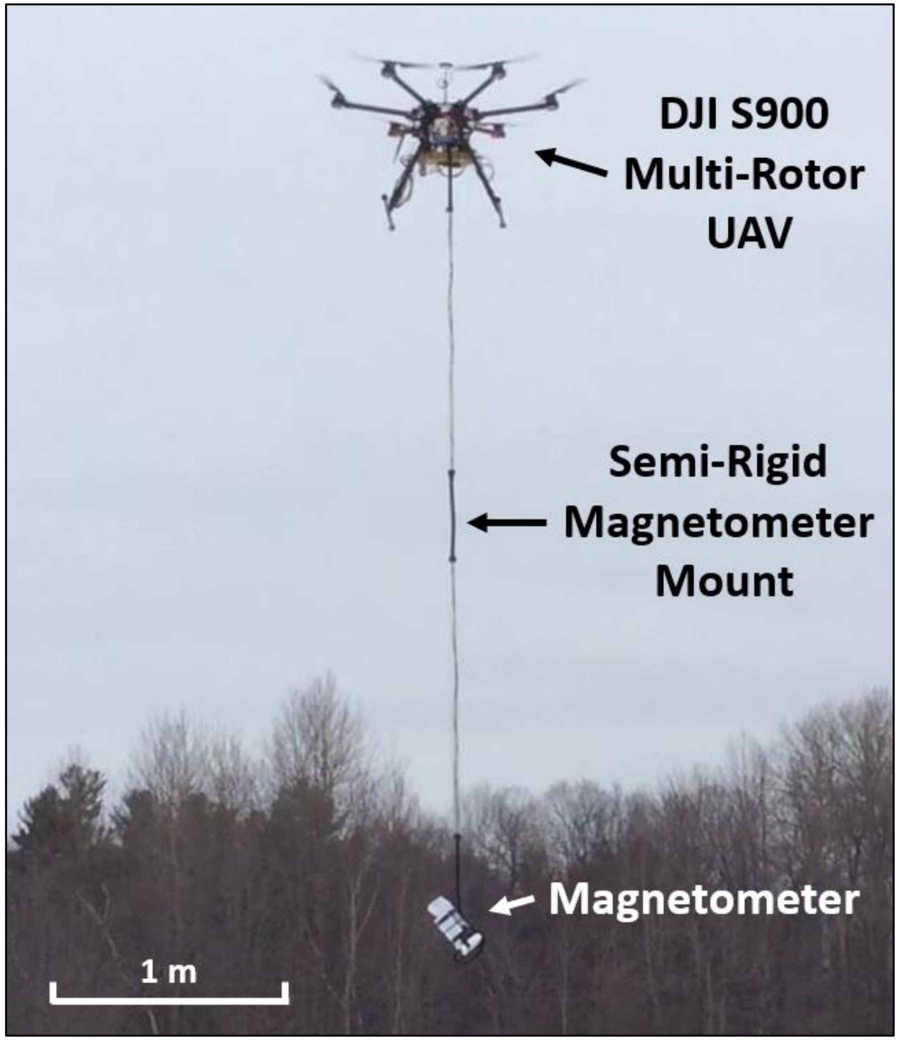

Walter et al. 2020

Measured Magnetometer Setback Distances

DJI S900: ~3m

(2.2 kg payload)

- Lighter & Smaller UAV
- Smaller Brushless Motors
- Smaller Solenoids
- Smaller Permanent Magnets

DJI Wind 4: ~5m

(2.2 kg payload)

- Heavier & Larger UAV
- Larger Brushless Motors
- Larger Solenoids
- Larger Permanent Magnets

Walter et al. 2020

UAV-Borne
Aeromagnetic System Specifications

DJI S900 Multi-Rotor UAV

Magnetometer Offset Distance: 3m

Payload Weight: 2.2 kg

Power Supply: 16000 mAh

Flight Endurance: ~15 minutes
(@16000 mAh & 2.2 kg payload)

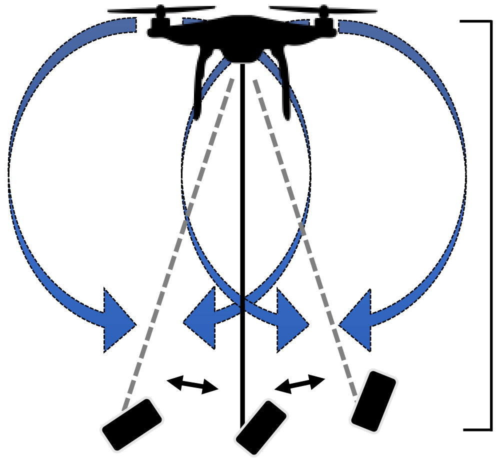

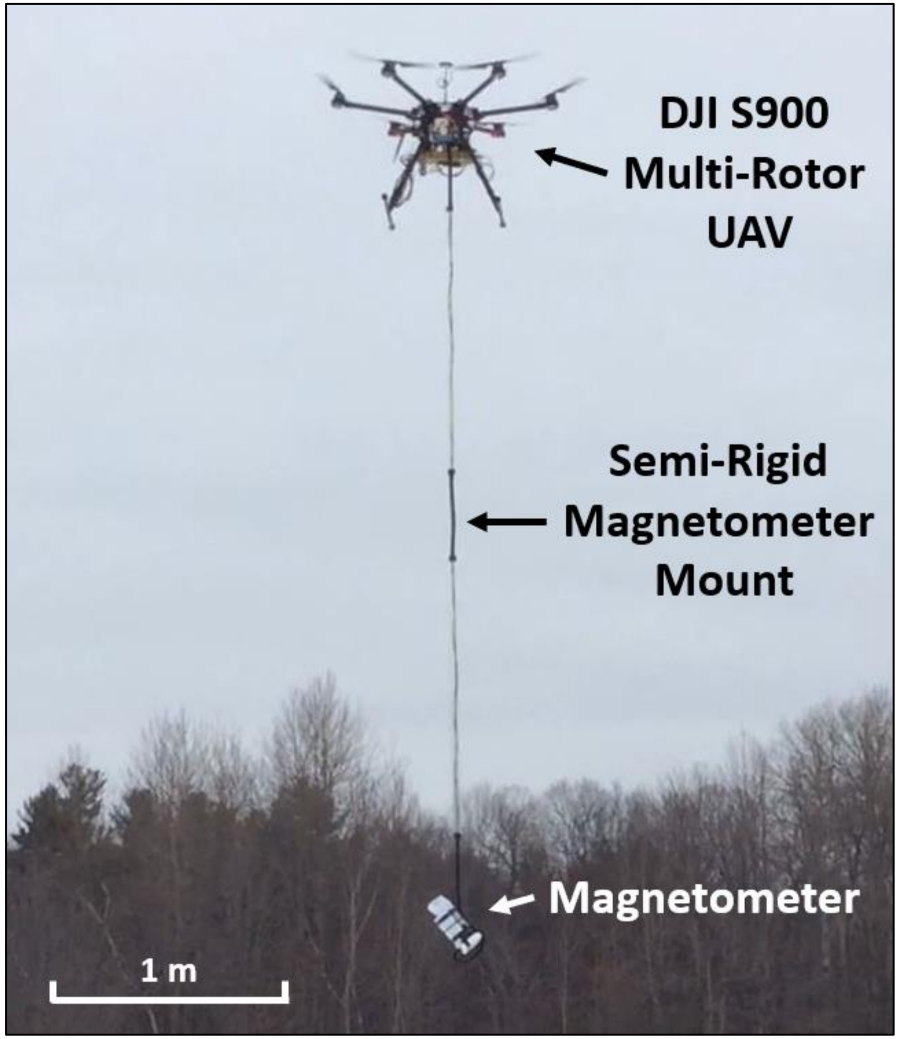

Walter et al. 2020

Data Acquisition System

GEM Systems: GSMP-35U
Potassium Vapour UAV
Magnetometer (10 Hz)

Ublox: EVK-7P
GPS
(10 Hz)

Lightware: SF-11
Laser Altimeter
(20 Hz)

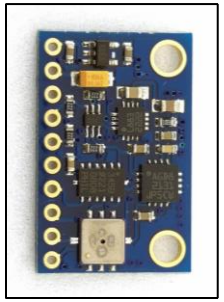

Adafruit: GY-80
10-DOF IMU
(80 Hz)

Total Payload Weight
2.2 Kg

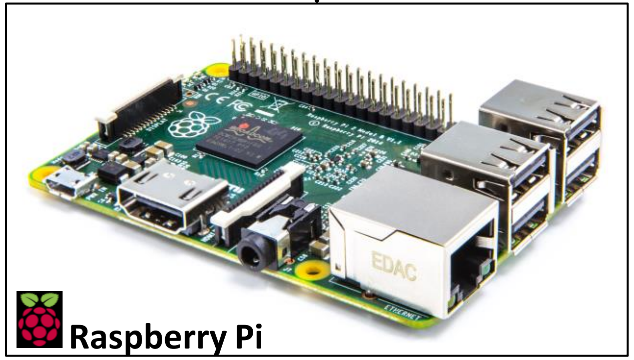

UAV-Borne Aeromagnetic Survey for Mineral Exploration

Flight Lines of Entire Survey

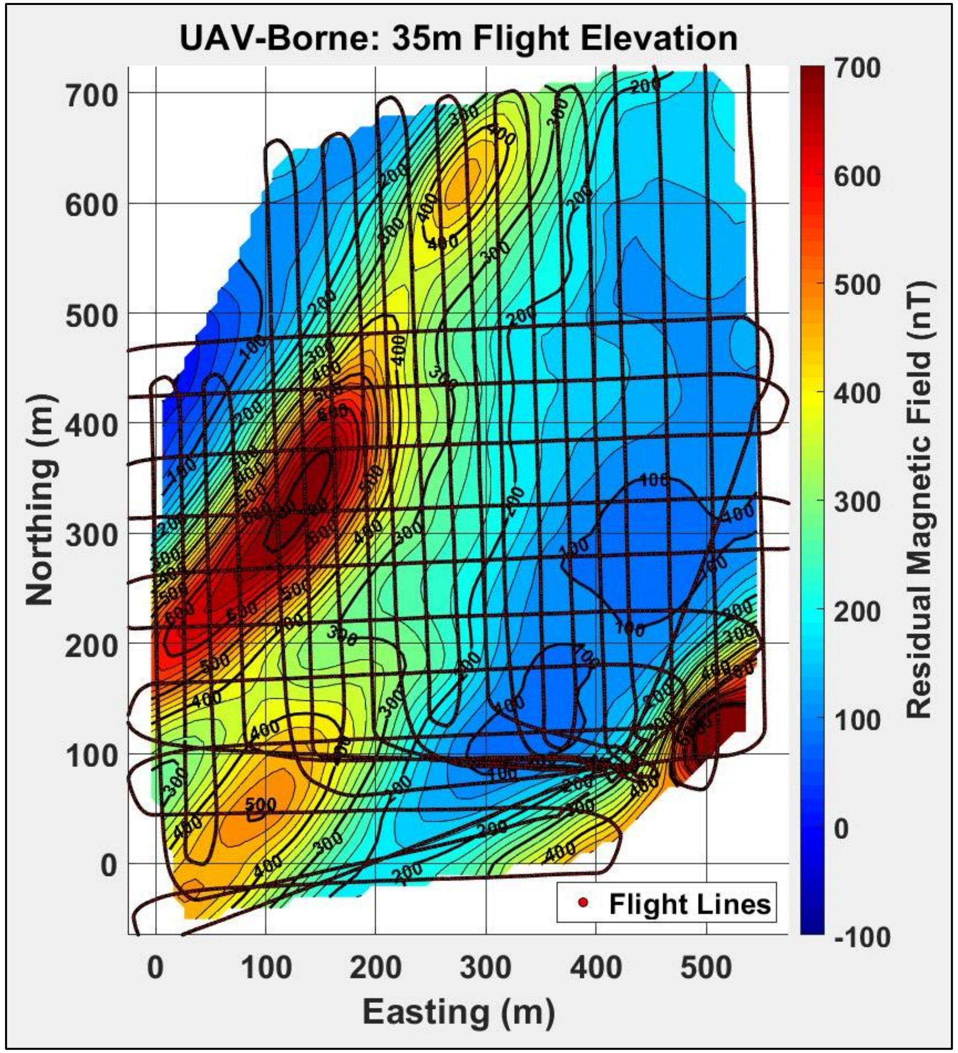

Flight Speed: 7 m/s

Selected Flight Lines for Study

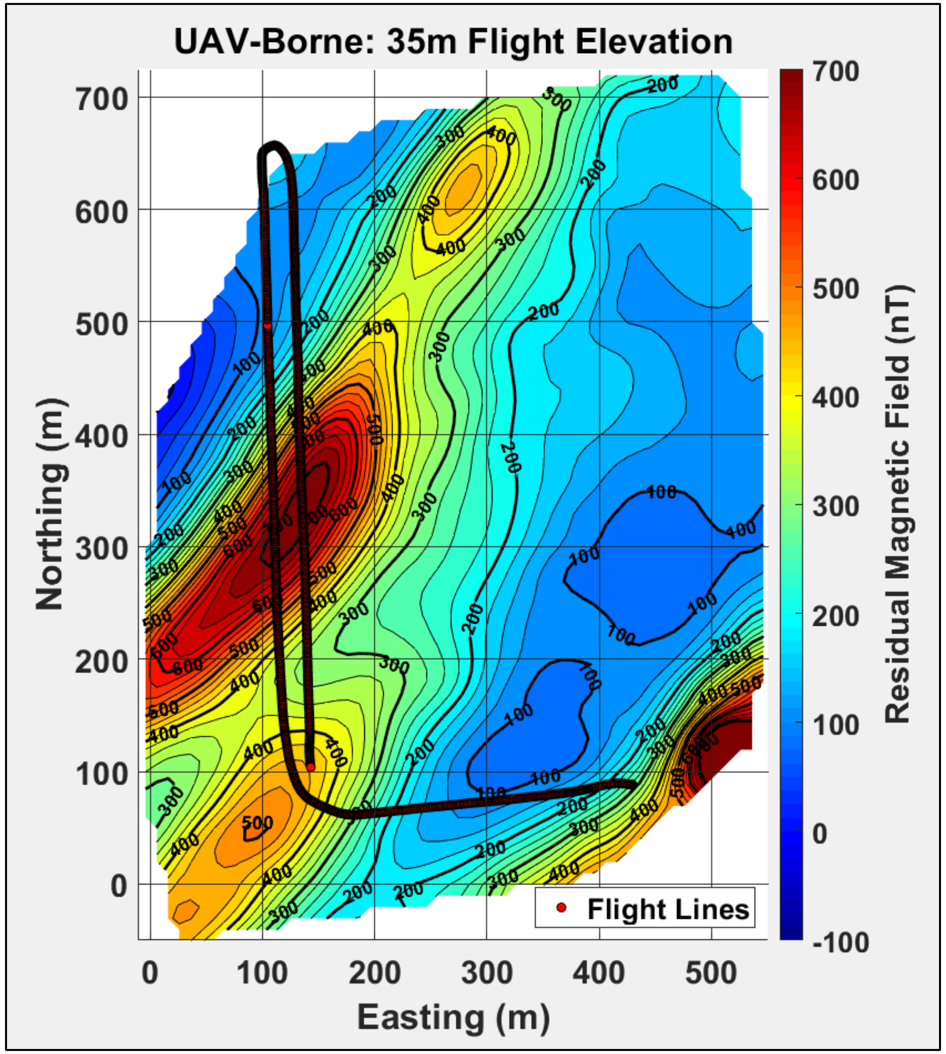

Overview of Selected Survey Lines And Flight Maneuvers

Hovering After Takeoff (A)

Approach Line

Wide Corner (50m radius) (B)

Flight Line 1

Sharp Corner 1 (12.5 m radius) (C)

Flight Line 2

Sharp Corner 2 (12.5 m radius) (D)

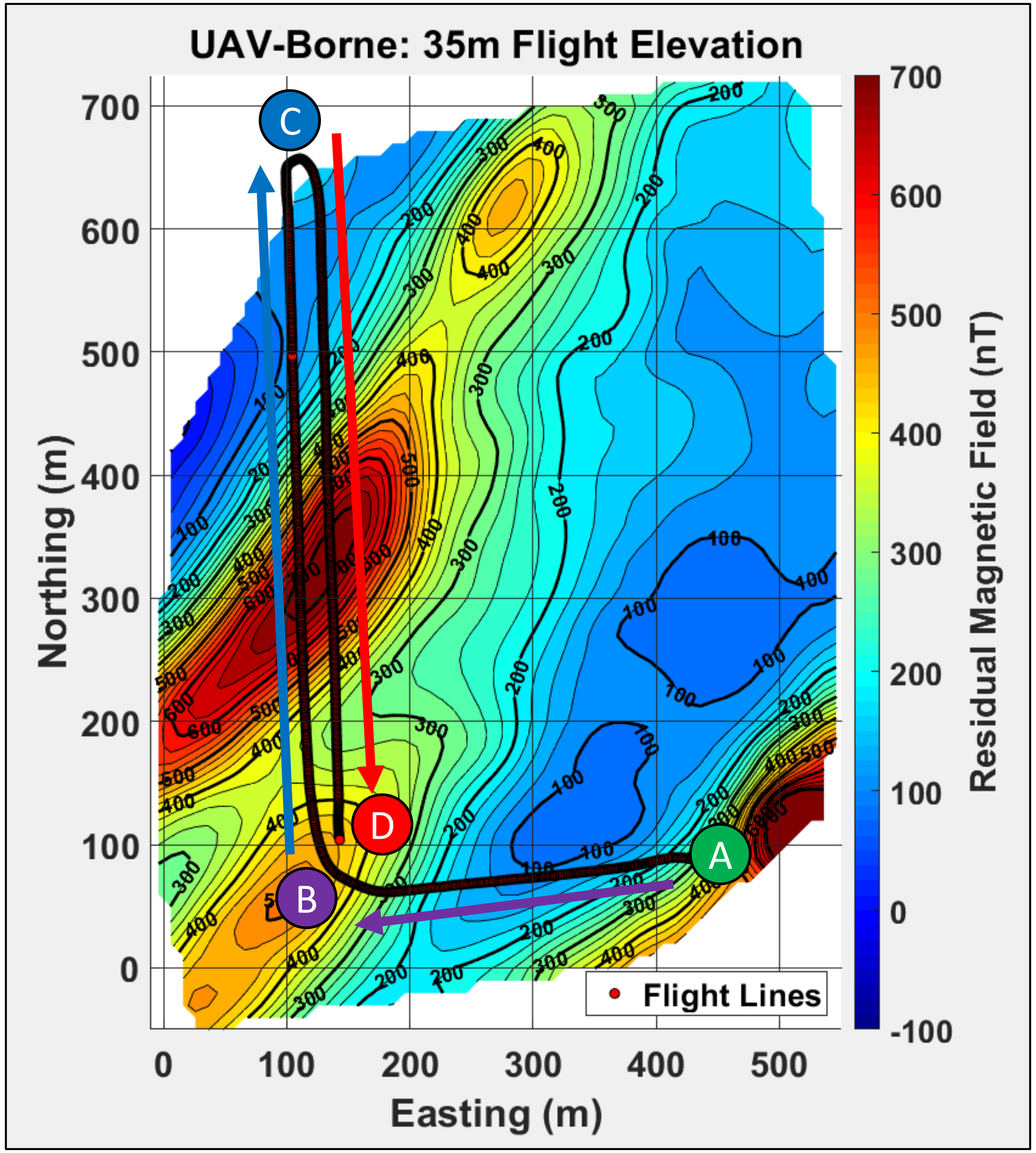

UAV-Borne
Residual Magnetic Field Data

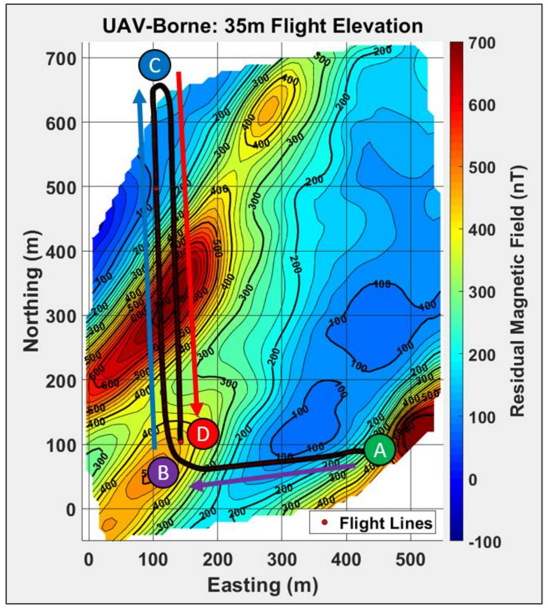

Hovering (A)

Wide Corner (B)

Sharp Corner 1 (C)

Sharp Corner 2 (D)

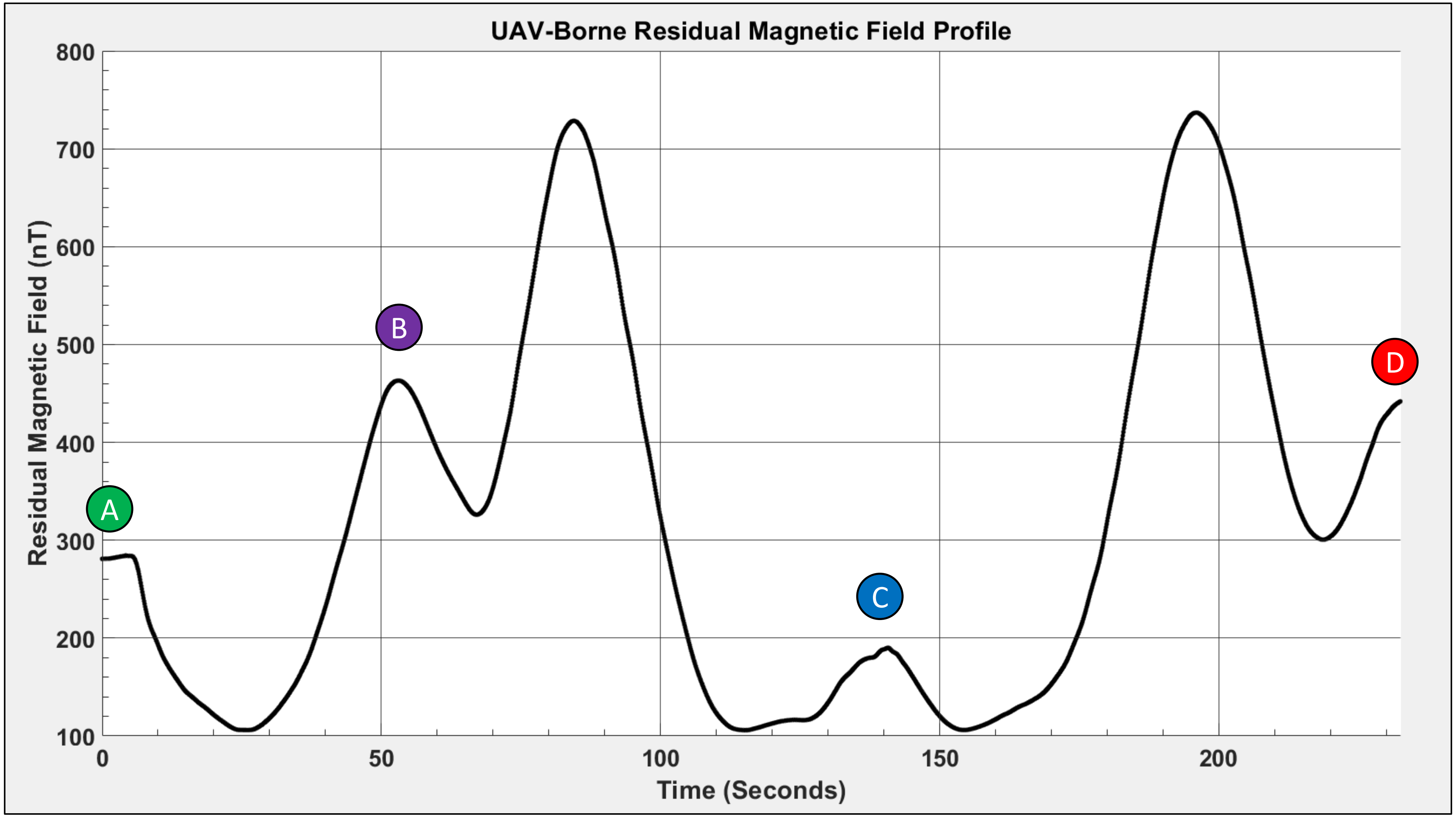

Walter et al. 2020

UAV-Borne Aeromagnetic Data Quality

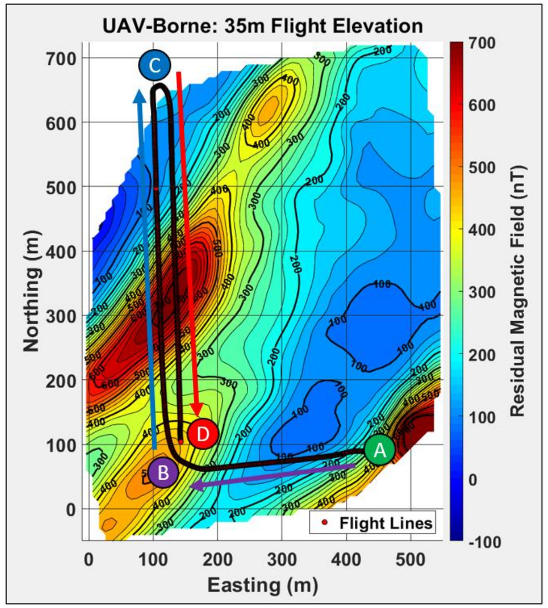

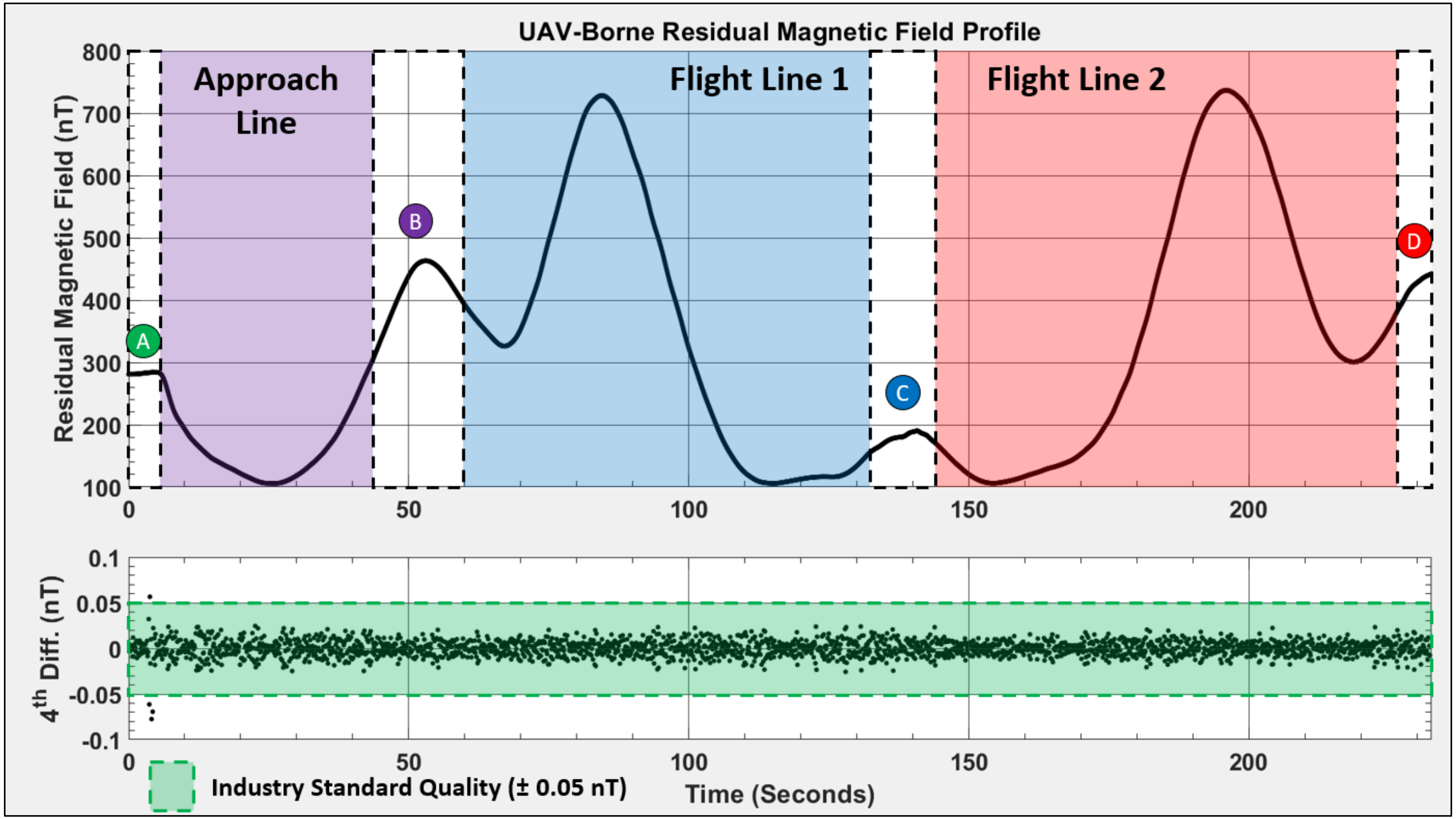

Hovering A

Wide Corner B

Sharp Corner 1 C

Sharp Corner 2 D

Walter et al. 2020

Frequency Domain UAV-Borne Residual Magnetic Field Data

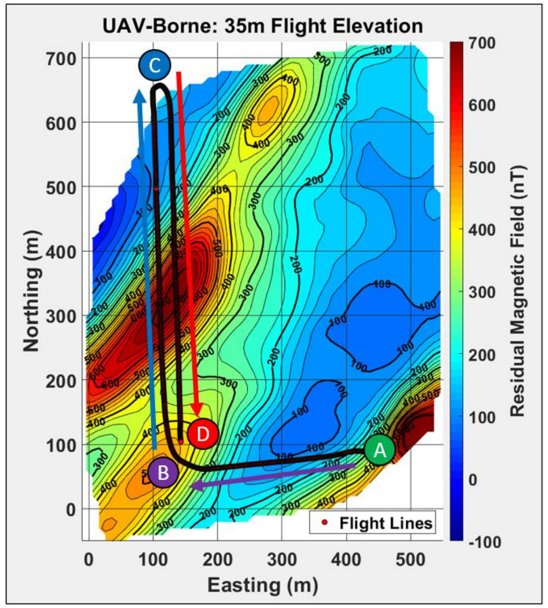

Swinging Frequency ~0.3 Hz

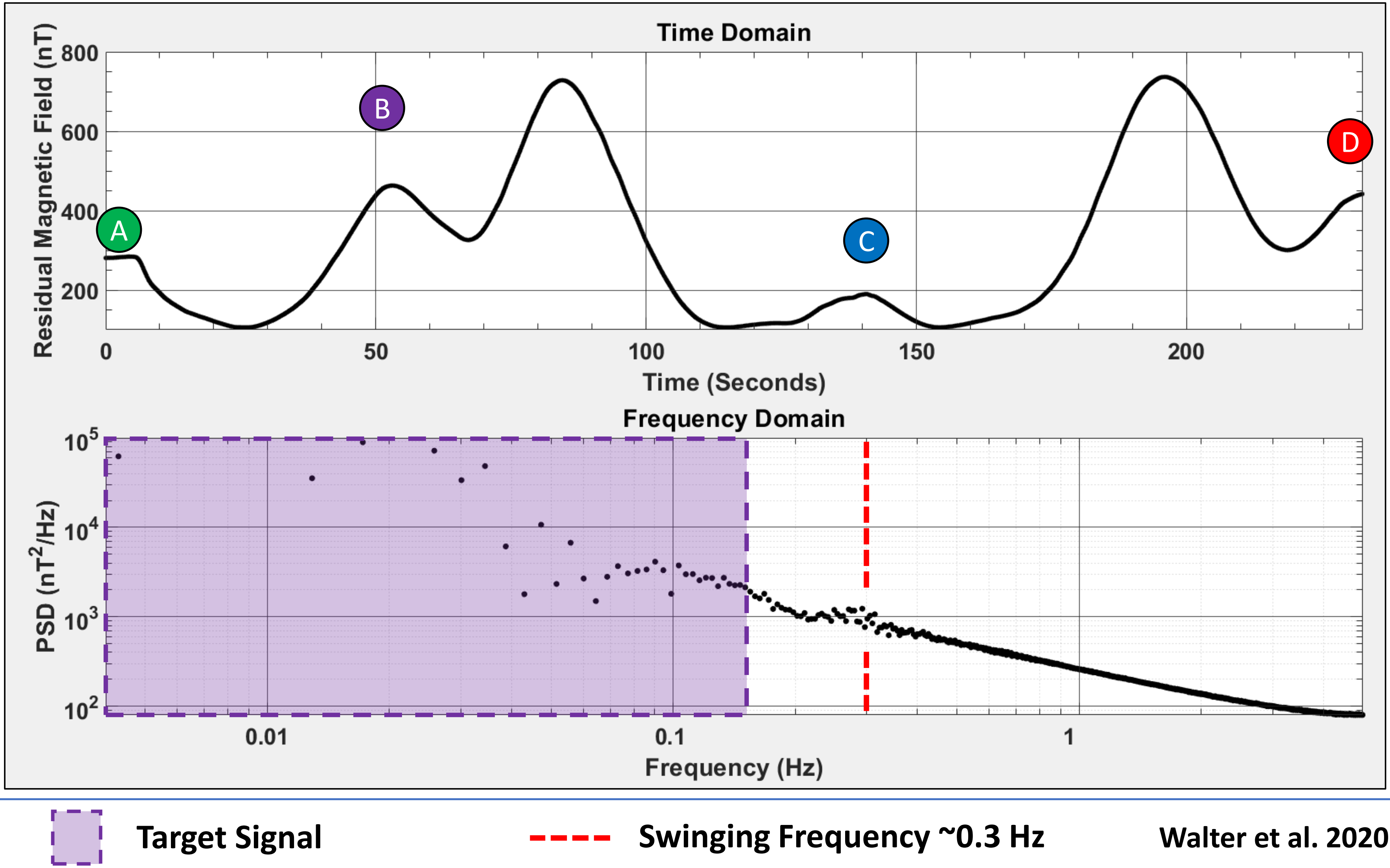

Walter et al. 2020

Spectrogram of UAV-Borne Residual Magnetic Field Data

Swinging Signal due to Cornering

High-Gradient Swinging Signal

Hovering (A)

Wide Corner (B)

Sharp Corner 1 (C)

Sharp Corner 2 (D)

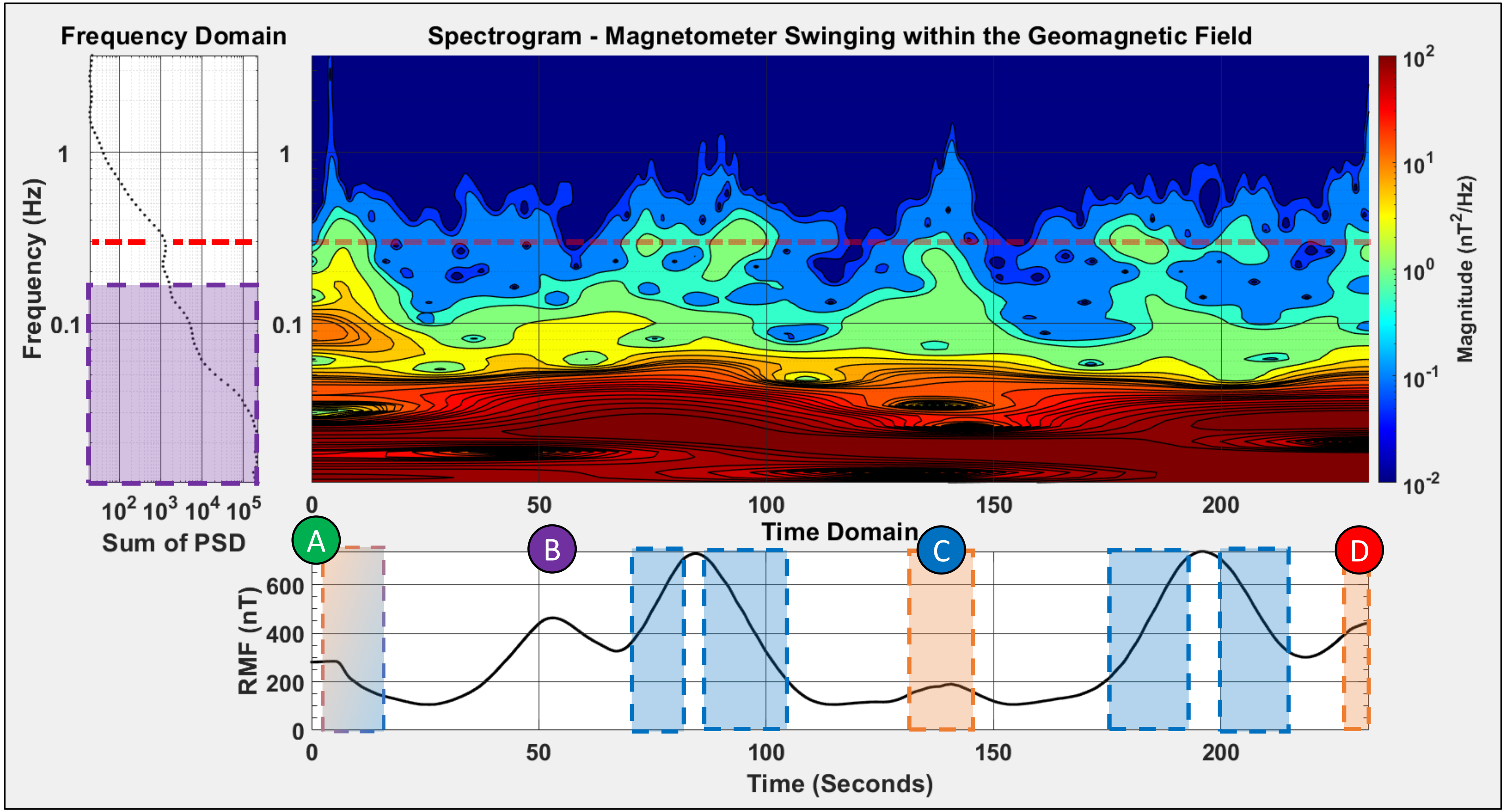

Target Signals

Swinging Frequency ~0.3 Hz

Walter et al. 2020

Isolated Magnetic Signal due to Magnetometer Swing

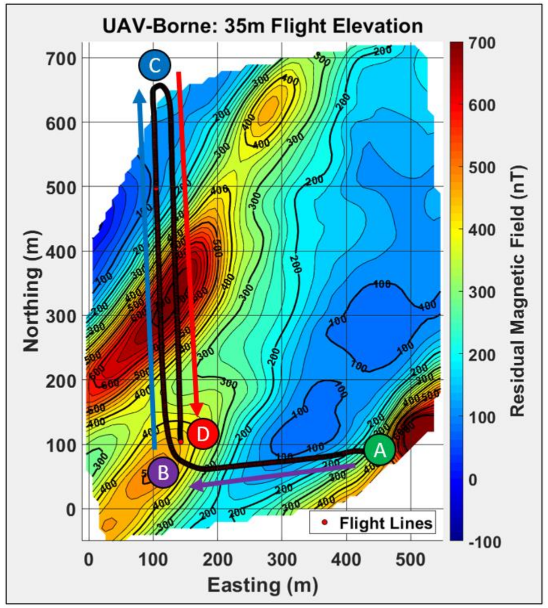

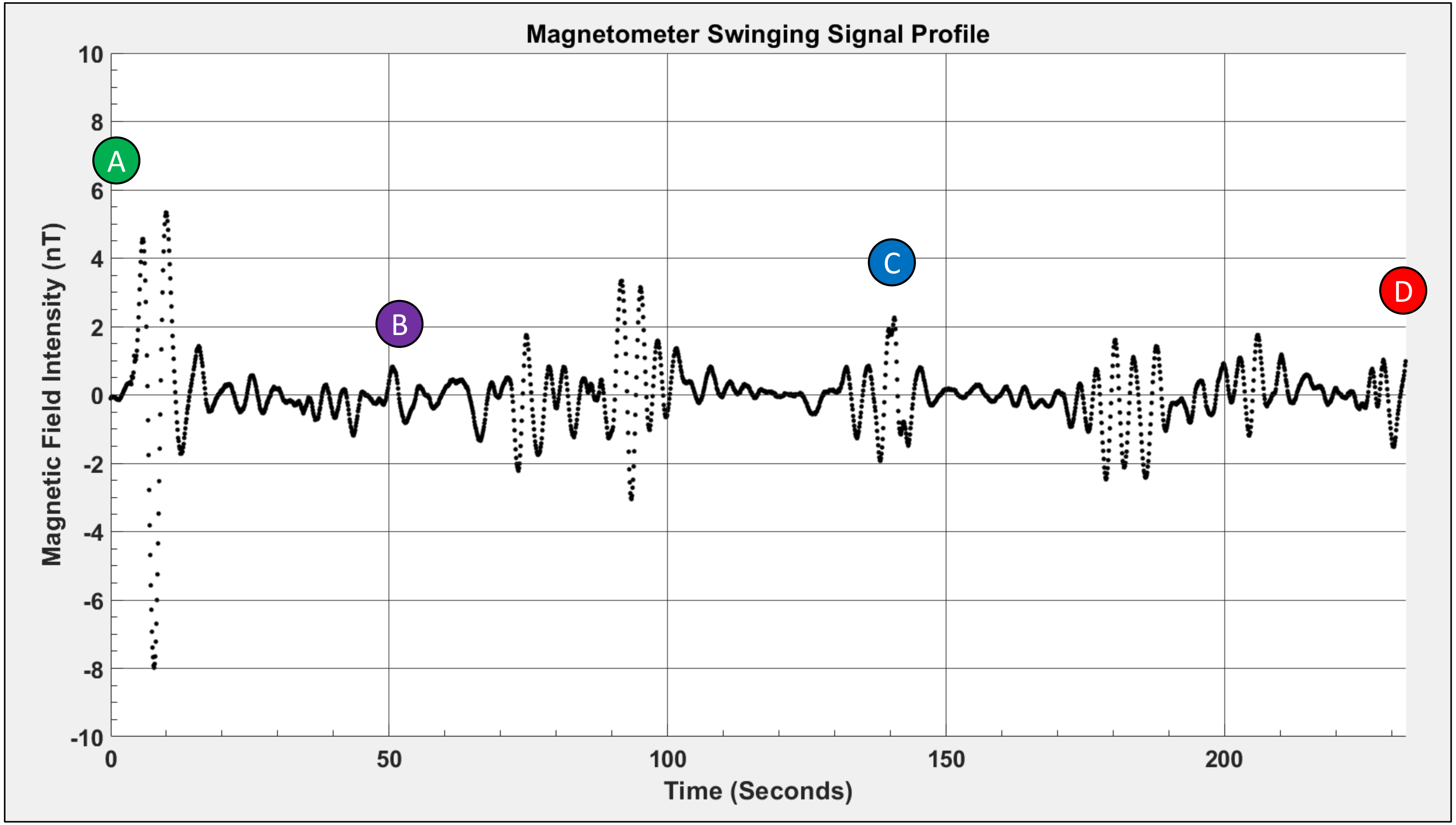

Hovering (A)

Wide Corner (B)

Sharp Corner 1 (C)

Sharp Corner 2 (D)

Walter et al. 2020

Isolated Magnetic Signal due to Magnetometer Swing

Swinging Signal due to Cornering

High-Gradient Swinging Signal

Hovering (A)

Wide Corner (B)

Sharp Corner 1 (C)

Sharp Corner 2 (D)

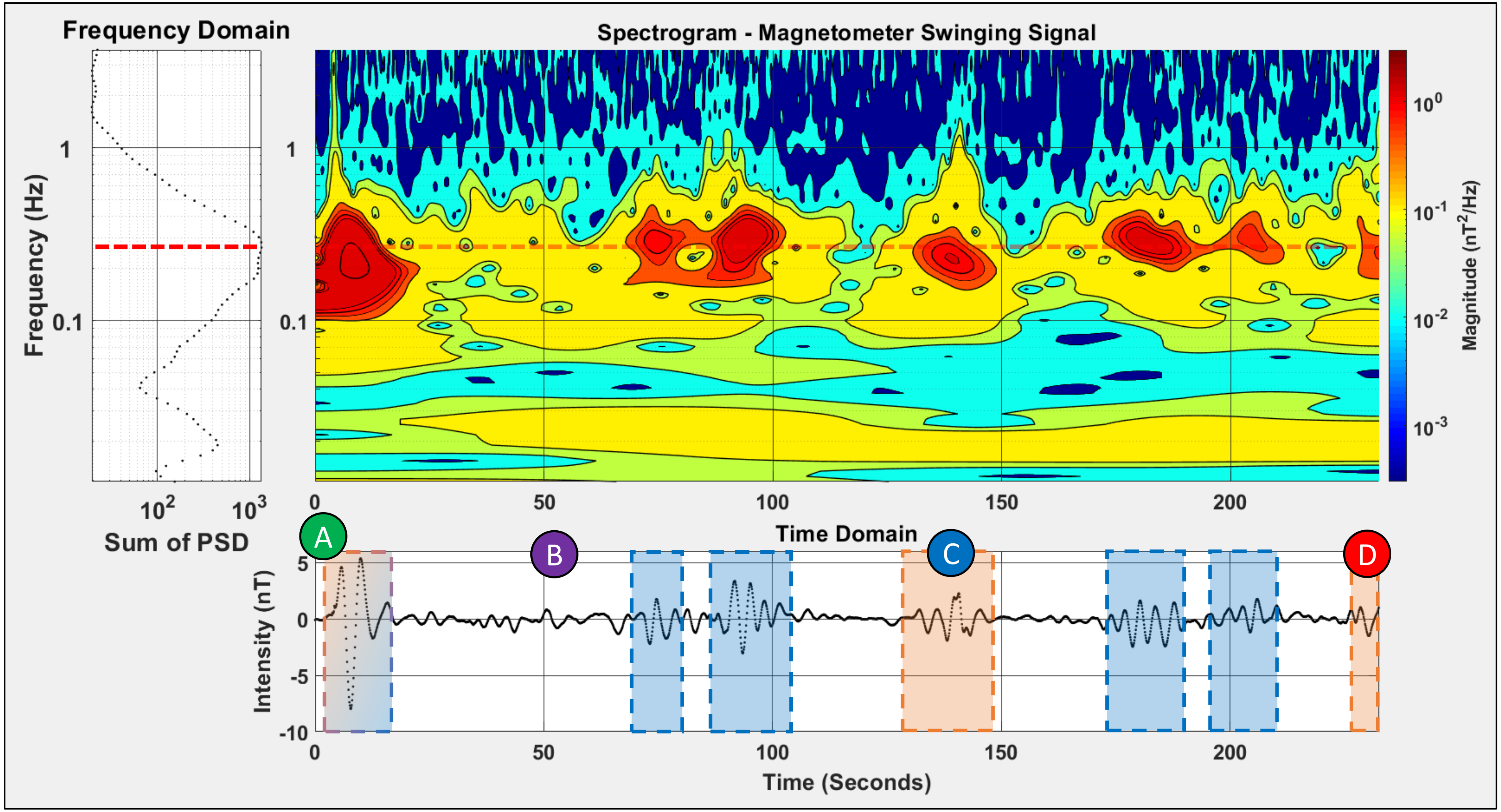

---- Swinging Frequency

Walter et al. 2020

IMU Roll Data of Magnetometer

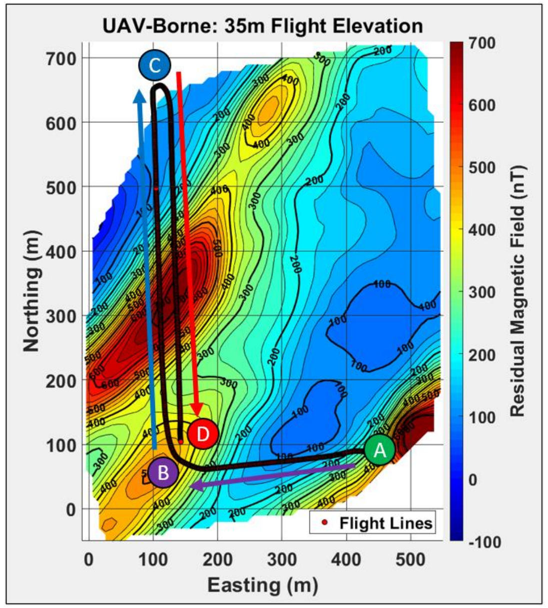

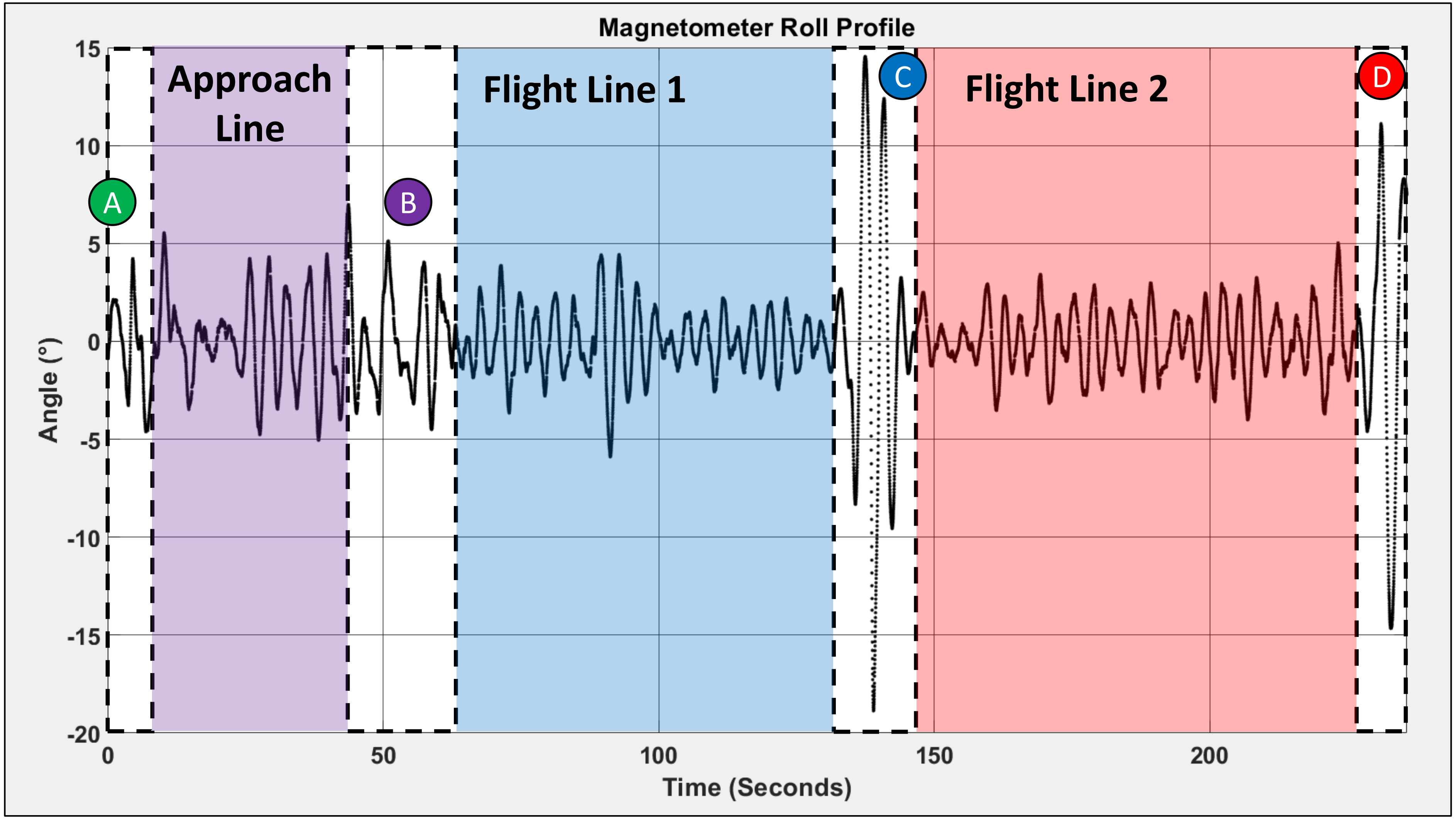

Hovering A

Wide Corner B

Sharp Corner 1 C

Sharp Corner 2 D

Walter et al. 2020

Frequency Domain IMU Roll Data

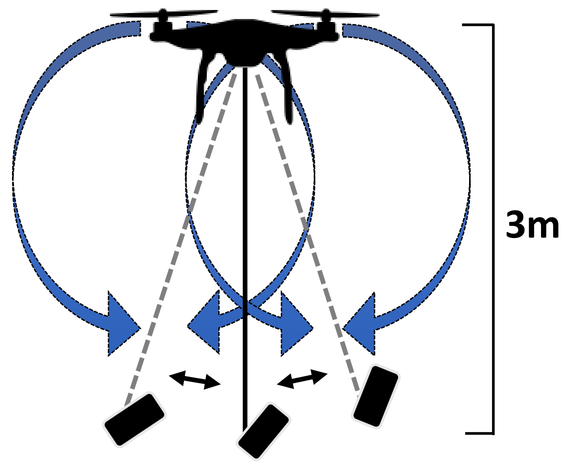

Swinging Frequency ~0.3 Hz

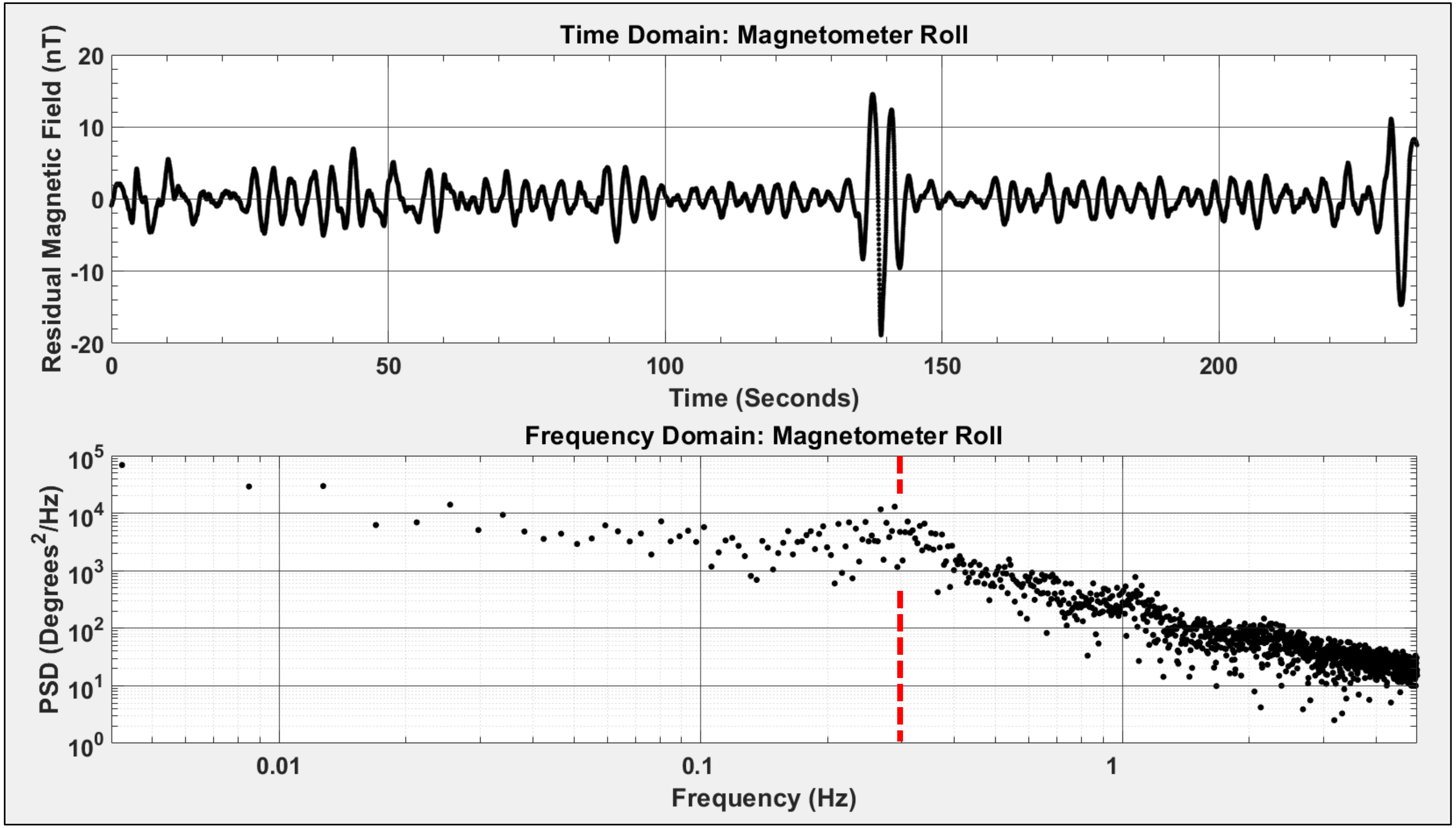

Walter et al. 2020

Frequency Domain Comparison of IMU Roll Data and Magnetometer RMI Data

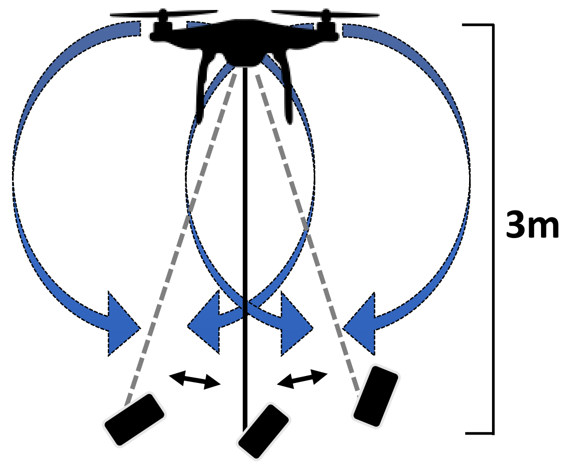

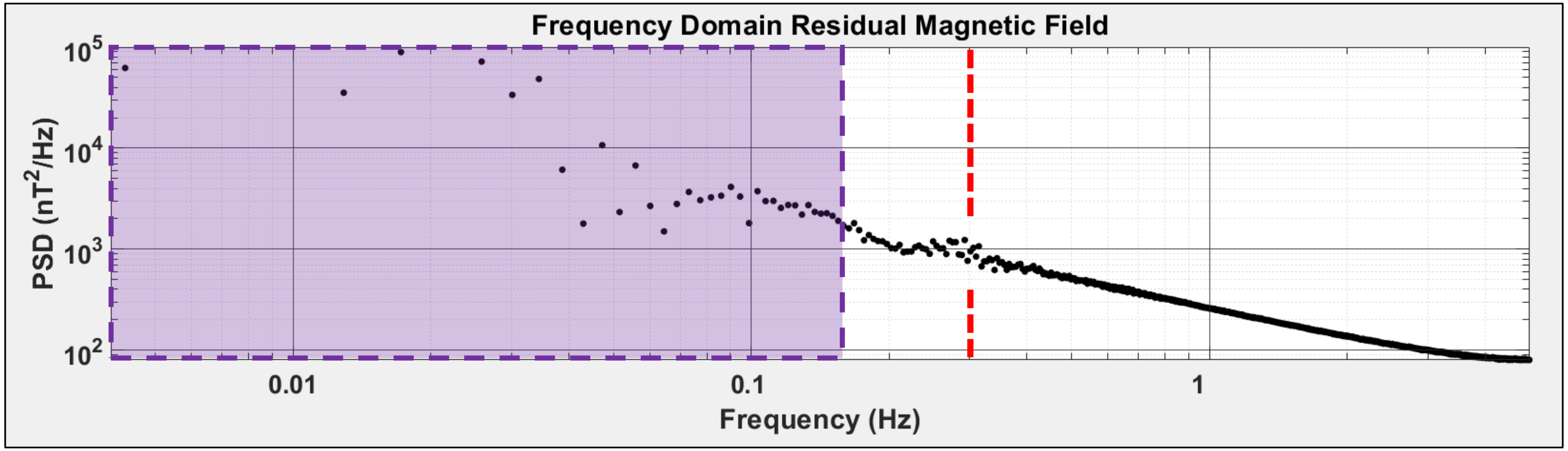

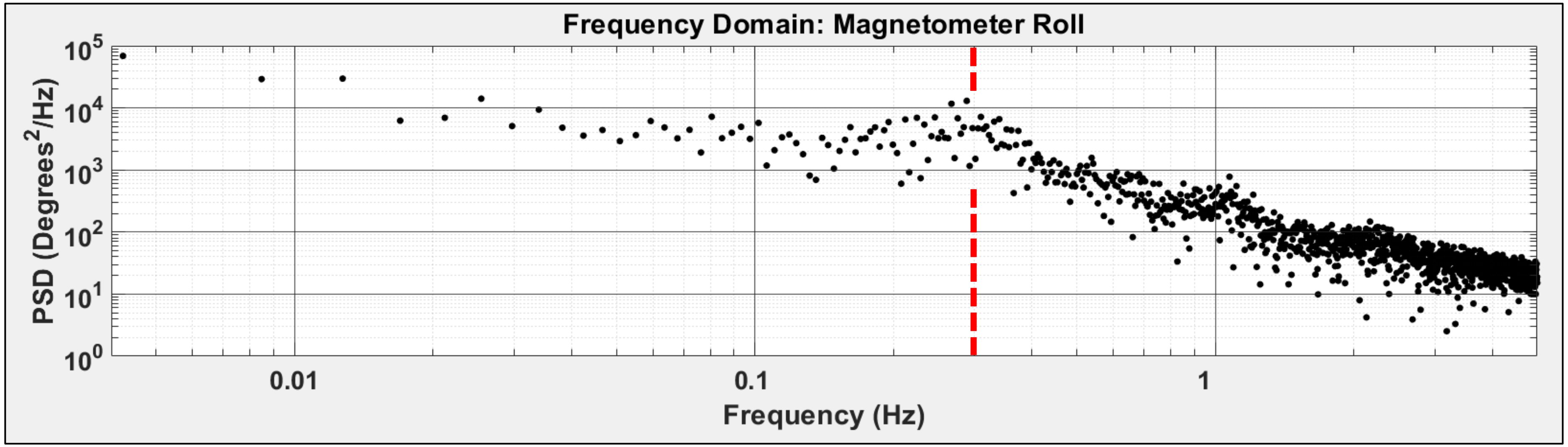

Target Signal

Swinging Frequency ~0.3 Hz

Walter et al. 2020

Spectrogram of Magnetometer Roll

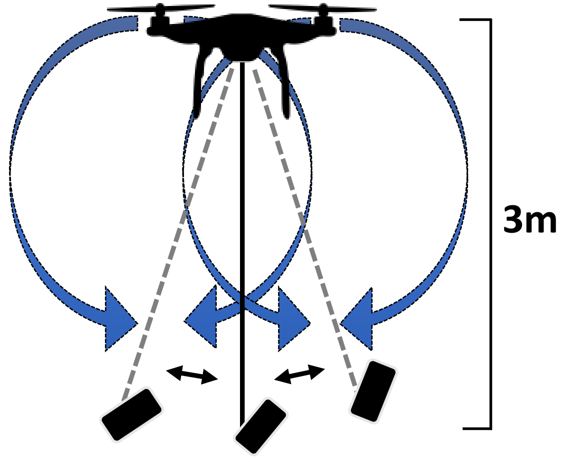

Swinging Signal due to Cornering

Hovering (A)

Wide Corner (B)

Sharp Corner 1 (C)

Sharp Corner 2 (D)

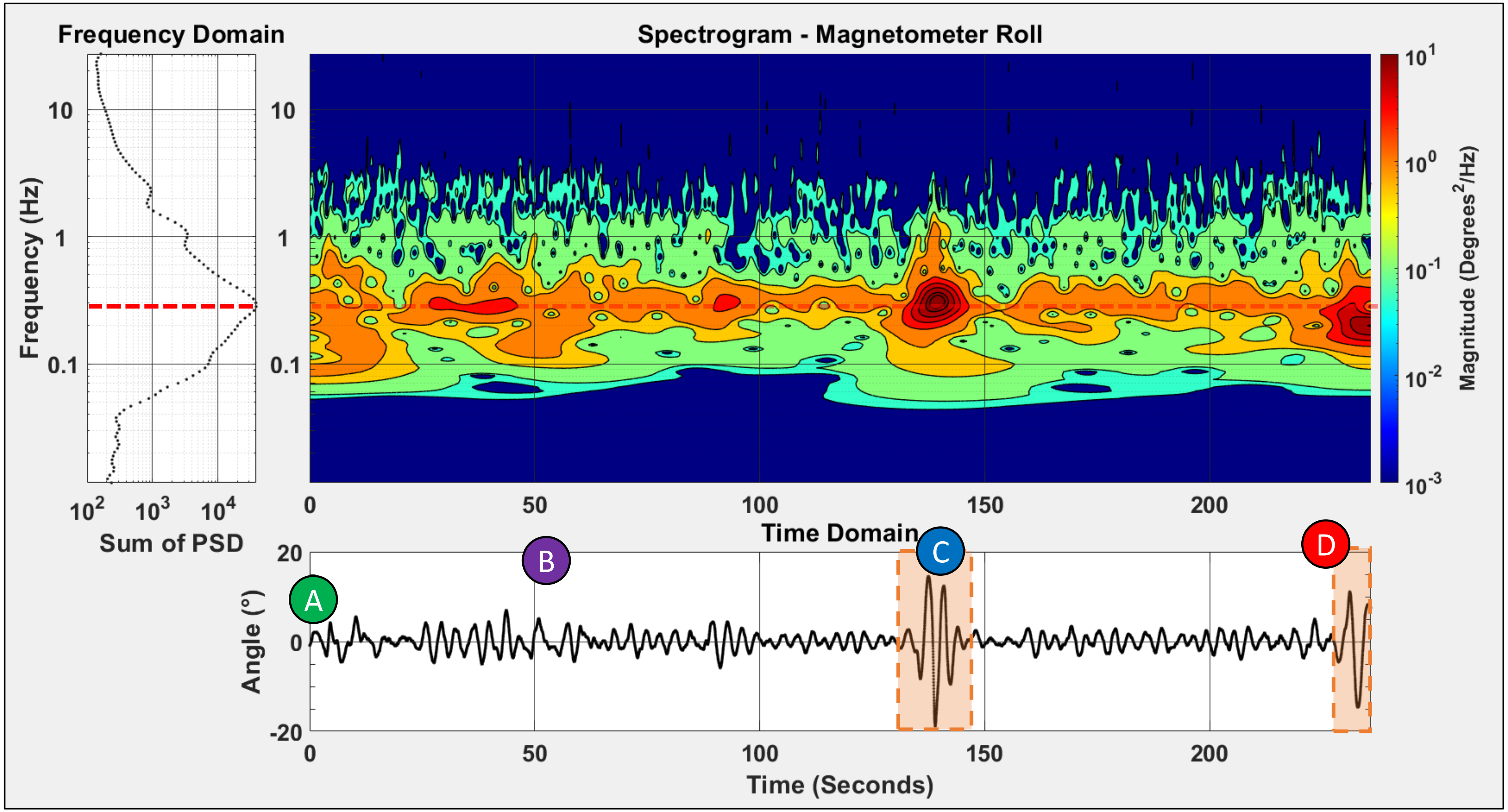

---- Swinging Frequency ~0.3 Hz

Walter et al. 2020

Applying a Low-Pass Filter to Remove Swinging Signals in Magnetic Data

Target Signal

Cut-off Frequency

Swinging Frequency

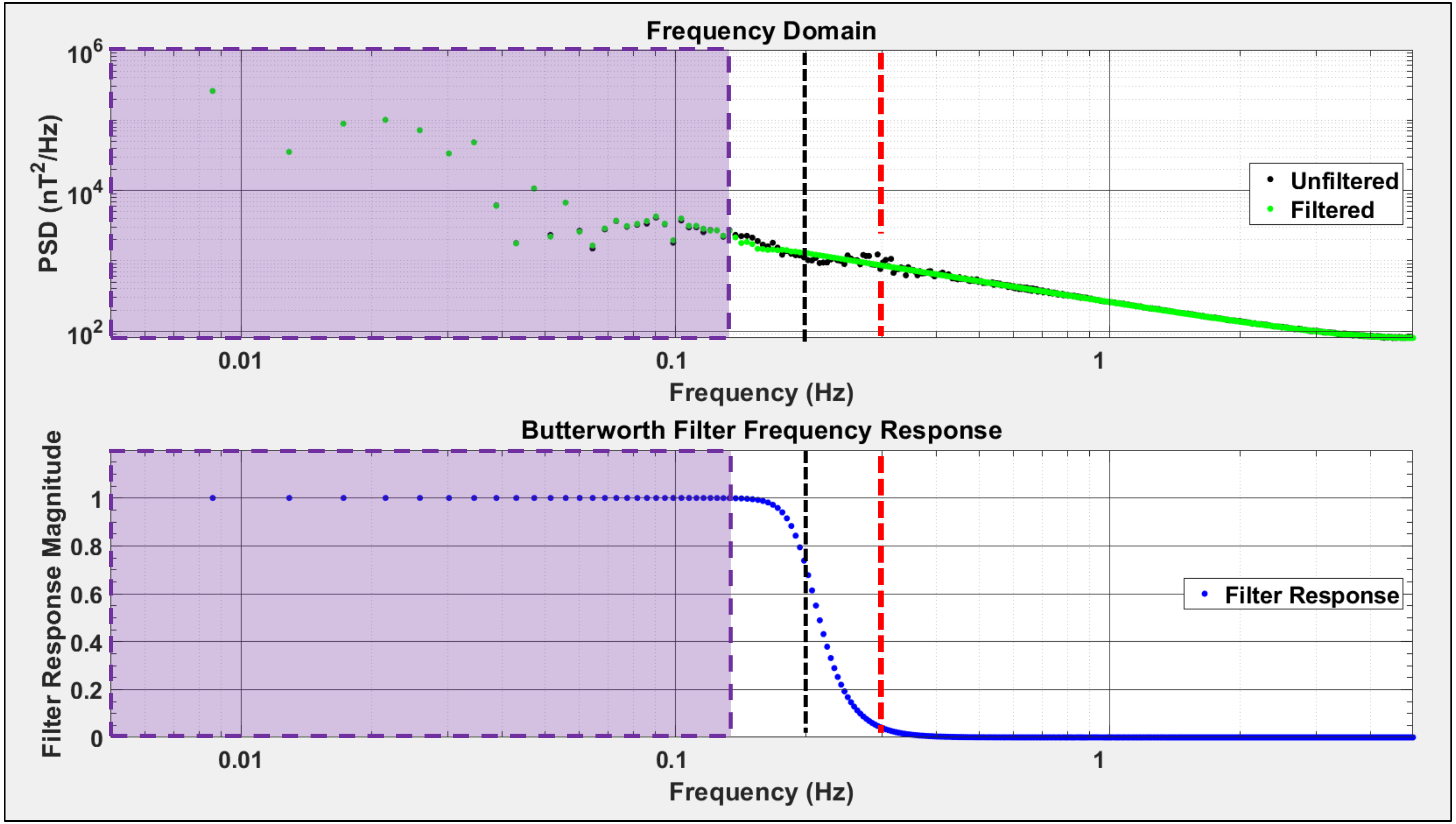

Walter et al. 2020

Spectrogram of Filtered Magnetic Field Data

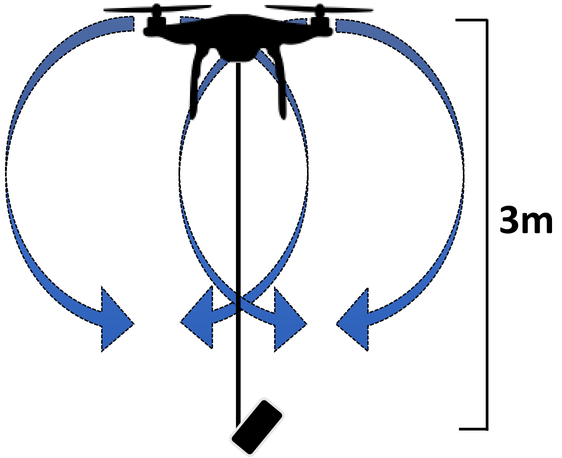

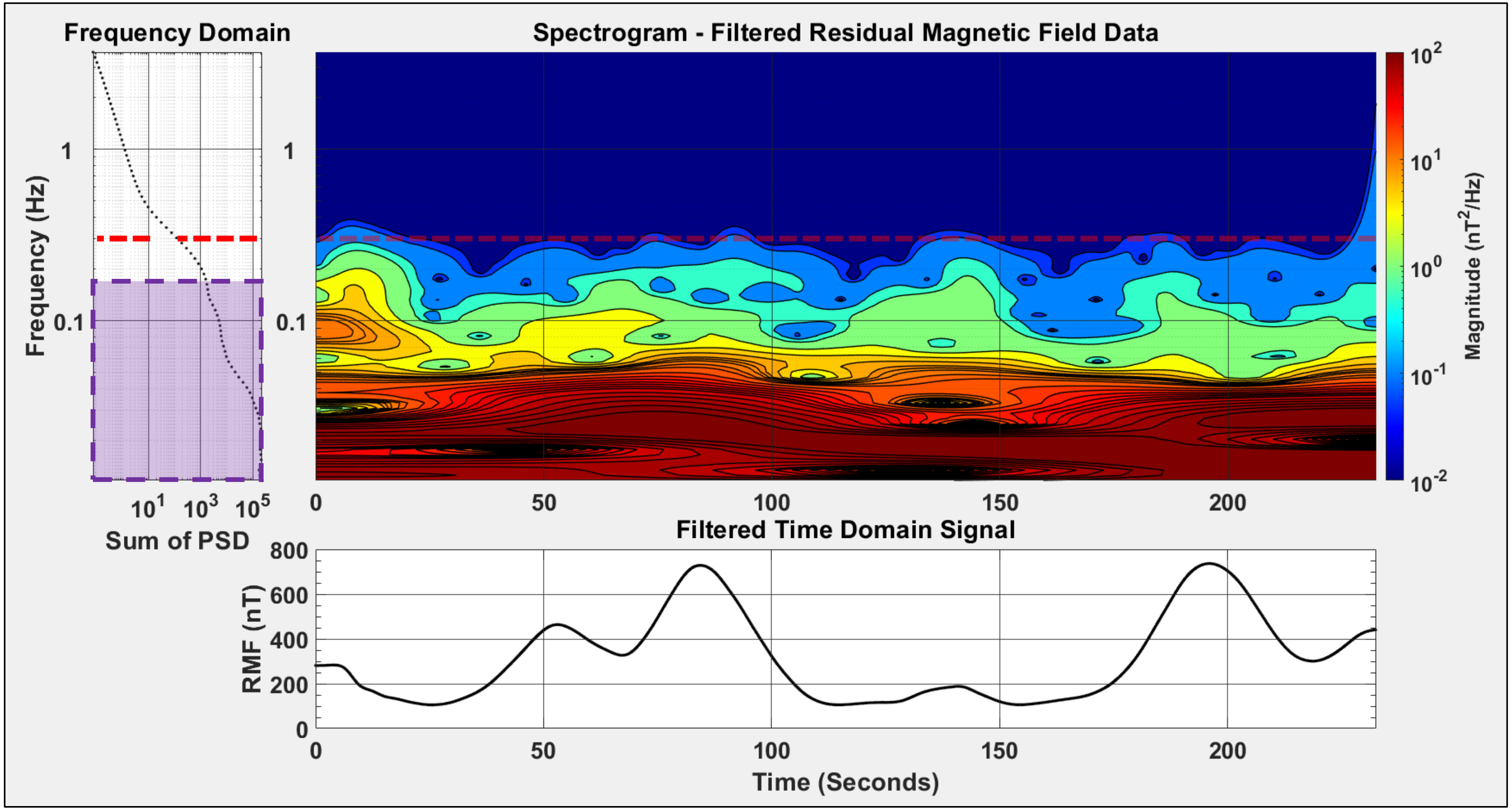

Target Signals

Swinging Frequency ~0.3 Hz

Walter et al. 2020

Filtered Magnetic Field Data

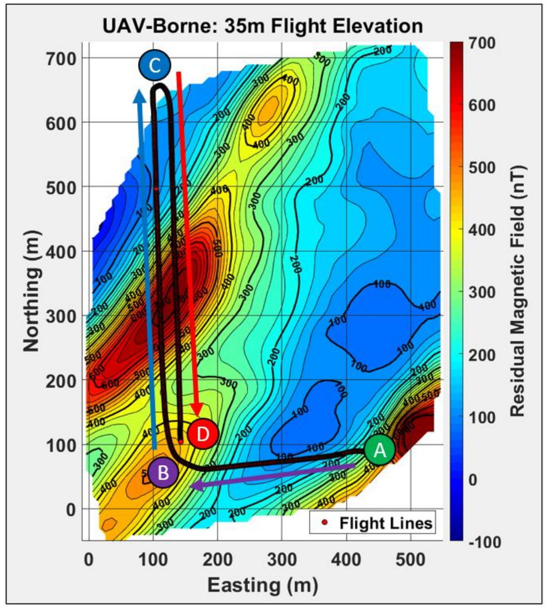

Hovering A

Wide Corner B

Sharp Corner 1 C

Sharp Corner 2 D

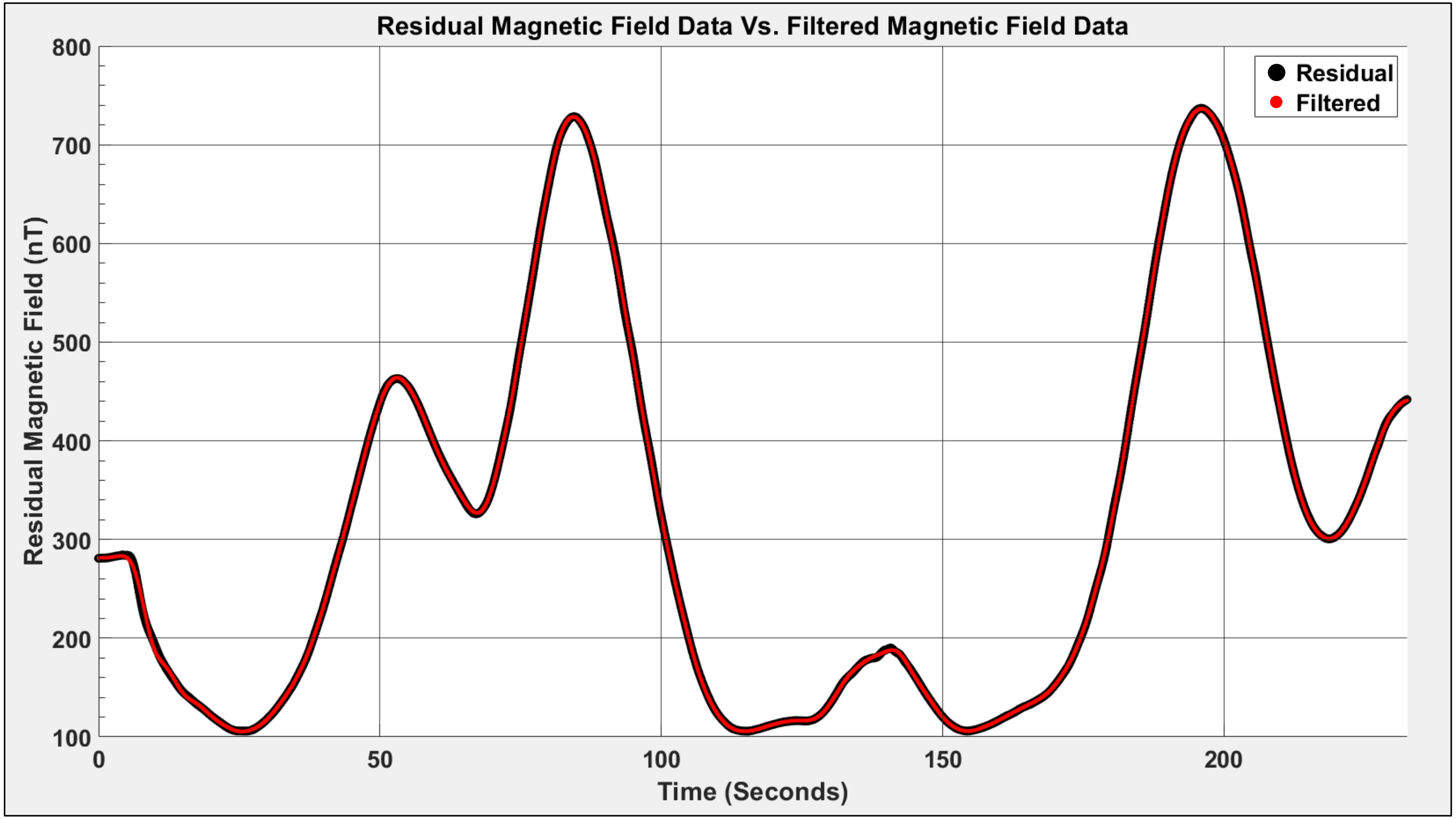

Walter et al. 2020

Conclusions

1. Magnetic signal amplitude of ~2 nT due to the swinging of the magnetometer in sharp corners. Represented in the magnetic data at C & D

2. Magnetic signal amplitude of ~3 nT due to the swinging of the magnetometer through a high-gradient geomagnetic field. Represented in the magnetic data at Flight Line 1 and Flight Line 2

3. Magnetic signal amplitude of ~5 nT due to the combine effect of a swinging magnetometer through a high-gradient geomagnetic field and the large acceleration experienced in pitch transitioning from hovering to traverse. Represented in the magnetic data in at A

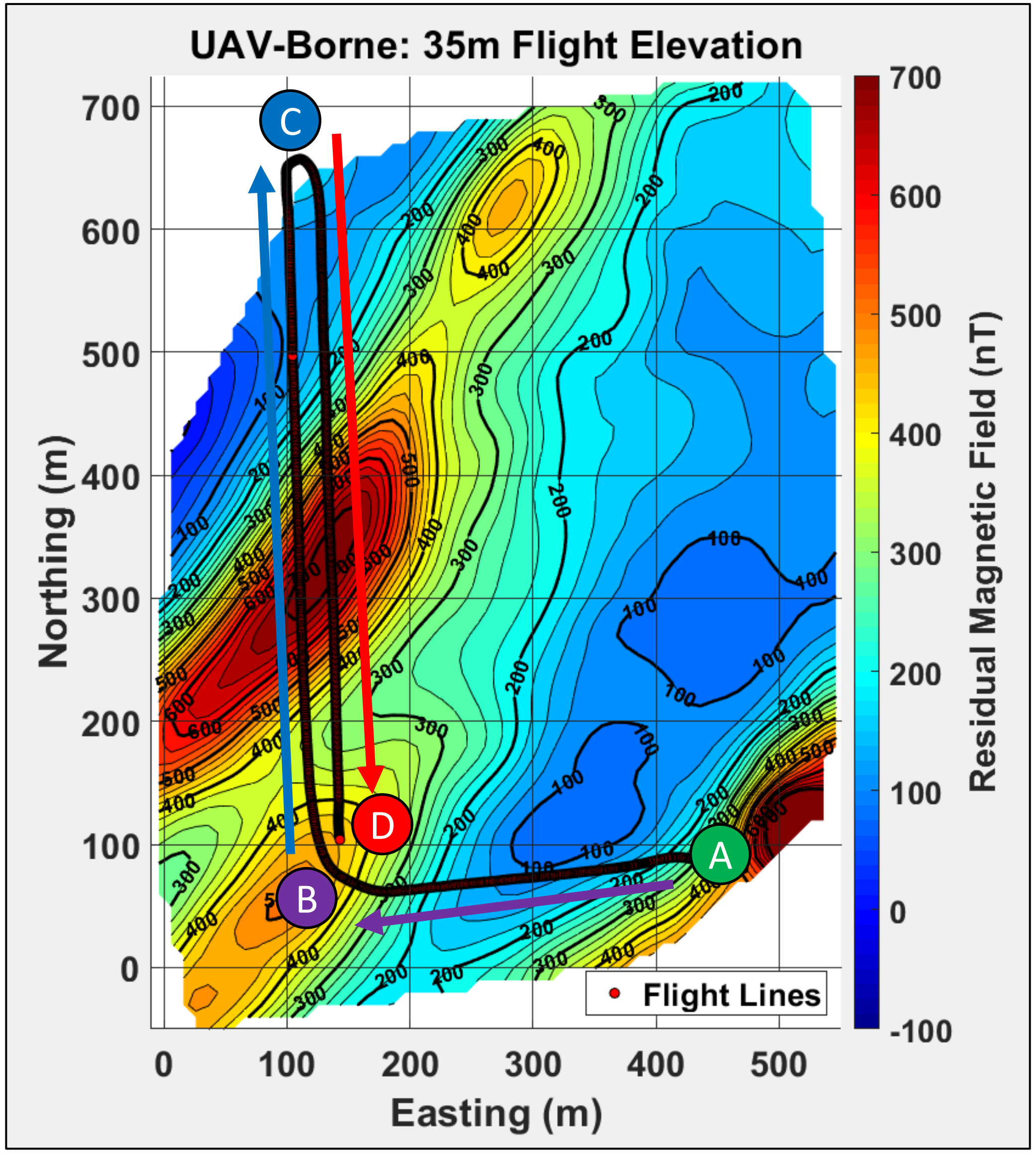

Conclusions

1. Magnetic signal amplitude of ~2 nT due to the swinging of the magnetometer in sharp corners. Represented in the magnetic data at C & D

2. Magnetic signal amplitude of ~3 nT due to the swinging of the magnetometer through a high-gradient geomagnetic field. Represented in the magnetic data at Flight Line 1 and Flight Line 2

3. Magnetic signal amplitude of ~5 nT due to the combine effect of a swinging magnetometer through a high-gradient geomagnetic field and the large acceleration experienced in pitch transitioning from hovering to traverse. Represented in the magnetic data in at A

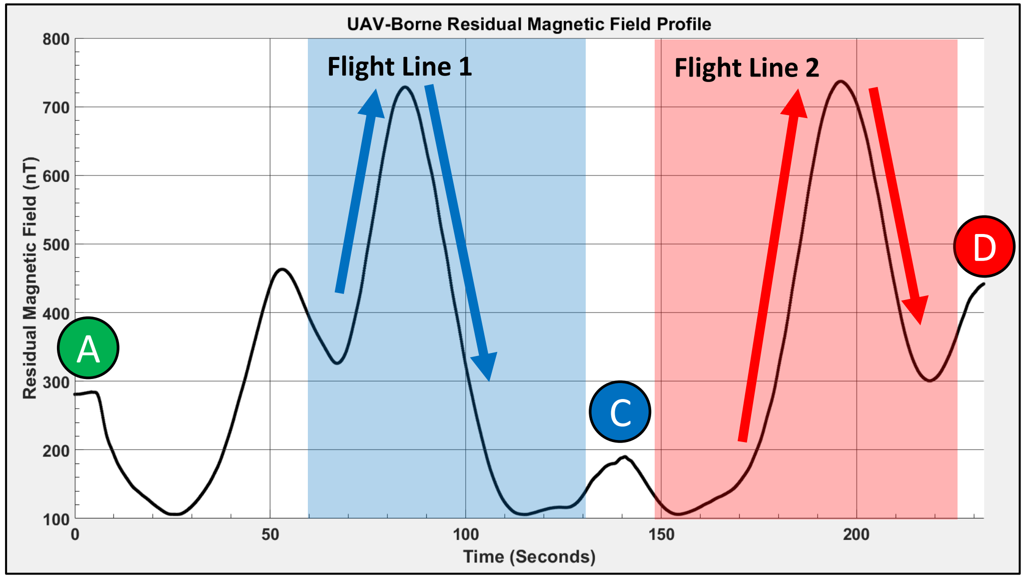

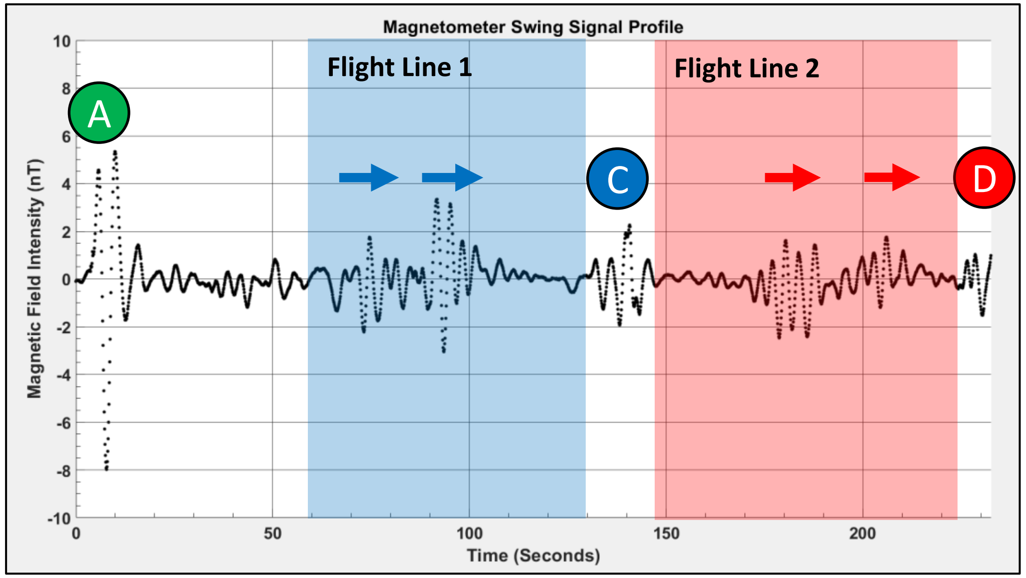

Conclusions

4. Magnetic signal amplitude of < 1 nT due to low amplitude swinging (< 10°) of the magnetometer through the low-gradient geomagnetic field. Represented in the magnetic data at position (B) during the wide turn

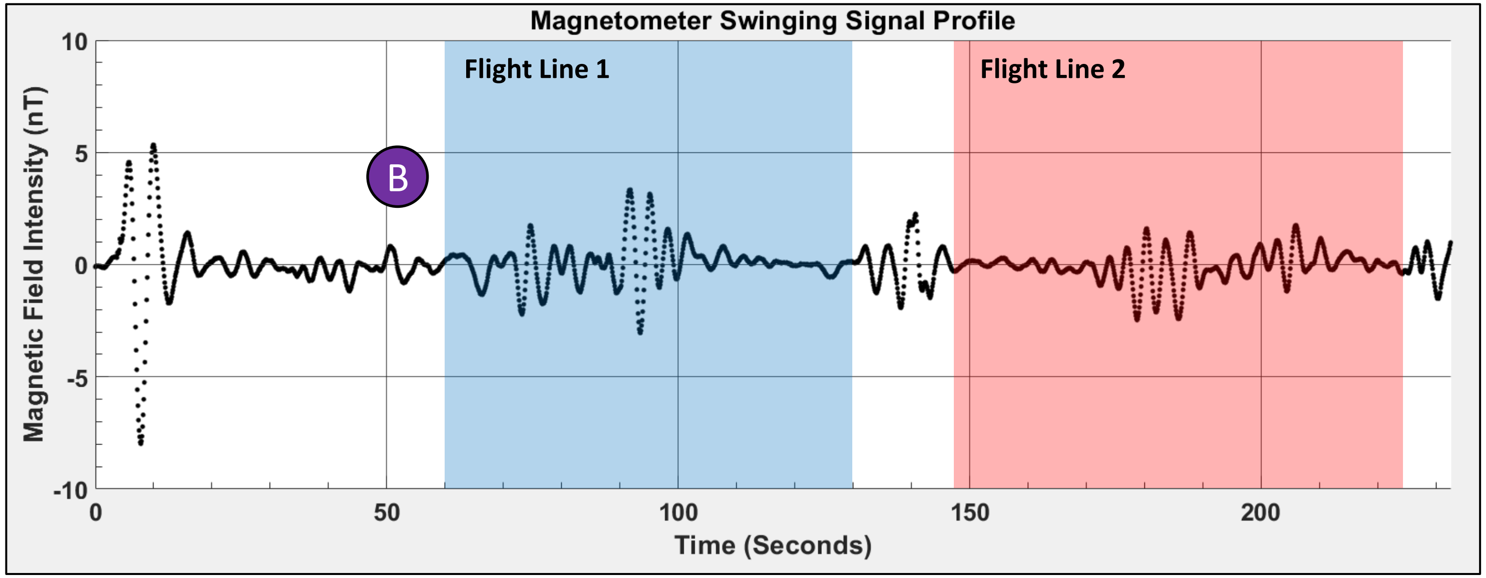

5. The swinging amplitude of the magnetometer in the roll axis down flight lines at a constant speed of 7.5 m/s is steady at ~ 5°. Represented in the magnetometer roll data at Flight Line 1 and Flight Line 2

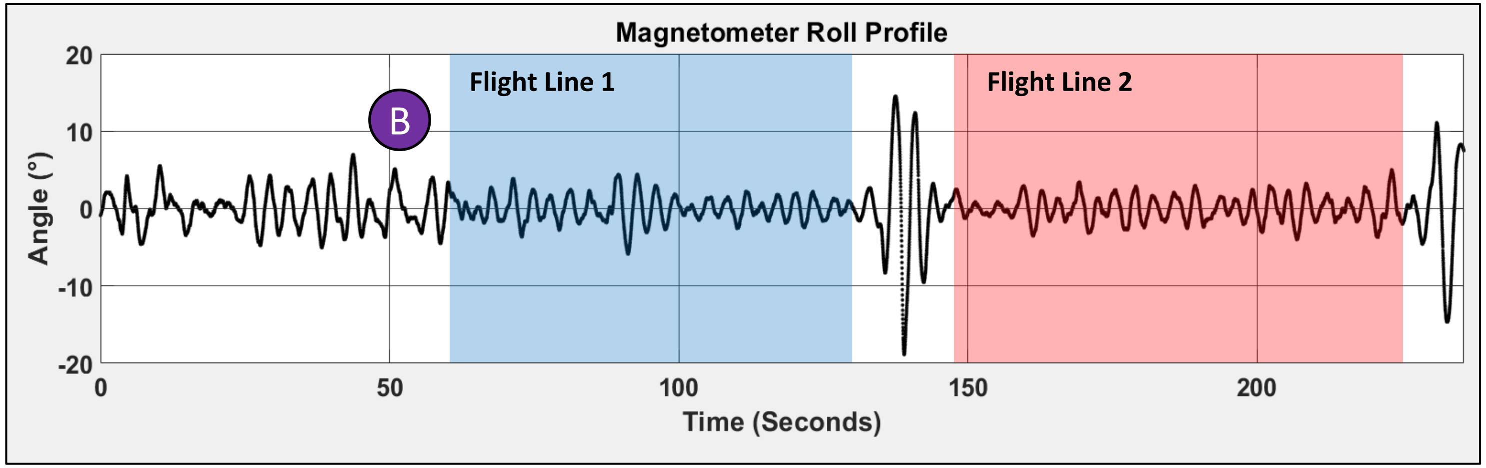

Walter et al. 2020

Conclusions

6. There are two, non-exclusive causes to the larger swinging signals: (1) swinging signal due to cornering or larger accelerations experienced by the magnetometer during flight maneuvers and (2) swinging signals due to magnetometer movement through larger-gradient geomagnetic field

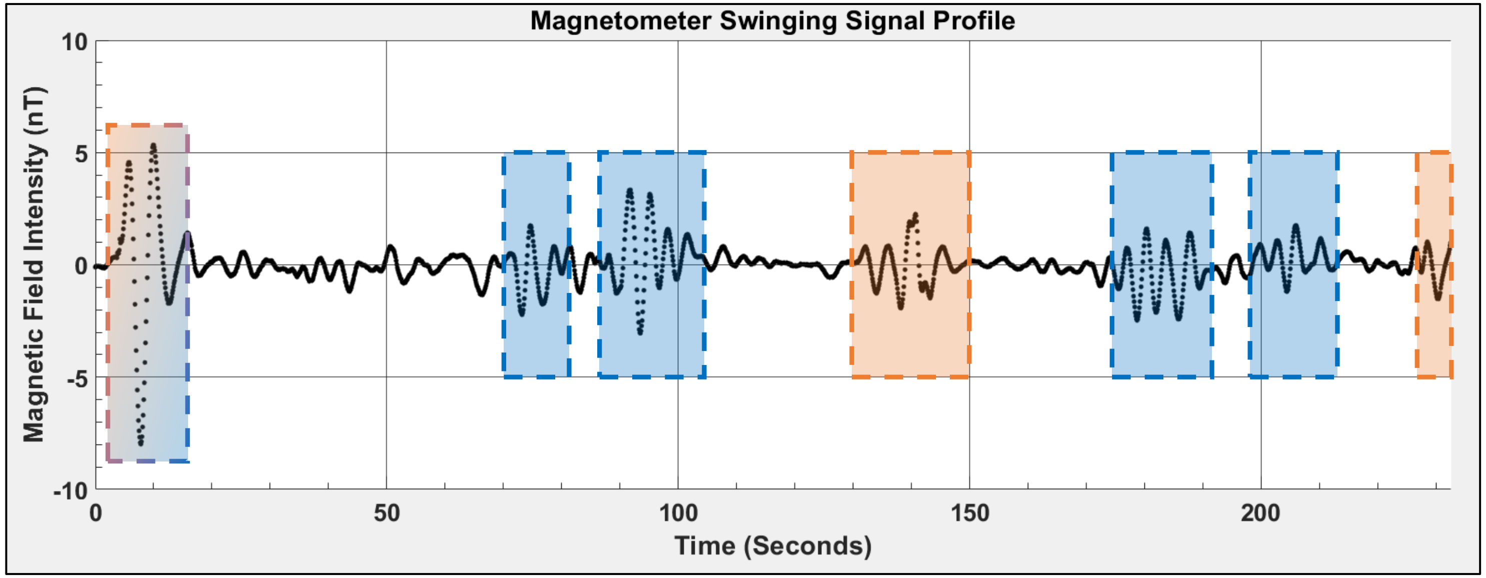

7. The ~0.3 Hz swinging signal in the RMI data were characterized and removed from the longer wavelength geological signals due to the two wavelengths not spectrally overlapping.

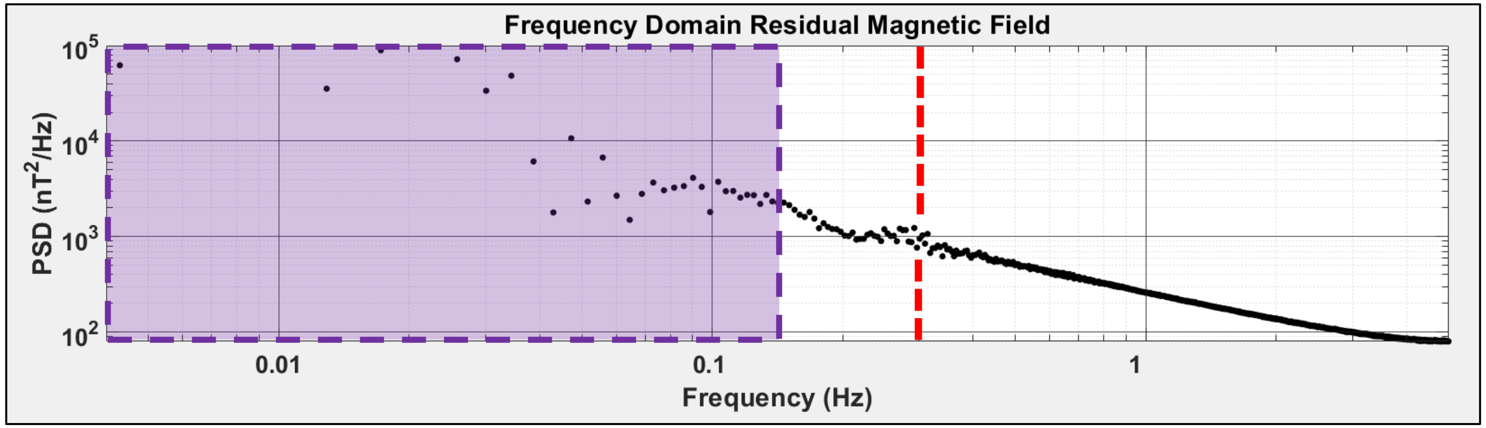

Target Signals

Swinging Frequency ~0.3 Hz

Walter et al. 2020

Works Cited

1. Walter C., Braun A. & Fotopoulos G. (2020) High-Resolution Unmanned Aerial Vehicle Aeromagnetic Surveys for Mineral Exploration Targets. *Geophysical Prospecting*, **68** (1), 334-349.
2. Walter C., Braun A. & Fotopoulos G. (2019) Impact of 3-D attitude variations of a UAV magnetometry system on magnetic data quality. *Geophysical Prospecting*, **67** (2), 465-479.

Acknowledgements